Systems/Circuits

A Visual Pathway into Central Complex for High-Frequency Motion-Defined Bars in *Drosophila*

Wenlan Duan (段文兰),[1,2*] Yihao Zhang (张艺豪),[1,2*] Xin Zhang (张鑫),[1,2*] Jihua Yang (杨继华),[1,2] Heying Shan (单鹤赢),[1] Li Liu (刘力),[1,2,3] and Hongying Wei (魏虹莹)[1,2]

[1]State Key Laboratory of Brain and Cognitive Science, Chinese Academy of Sciences Center for Excellence in Biomacromolecules, Institute of Biophysics, Chinese Academy of Sciences, Beijing 100101, China, [2]College of Life Sciences, University of the Chinese Academy of Sciences, Beijing 100039, China, and [3]Chinese Academy of Sciences Key Laboratory of Mental Health, Beijing 100101, China

Relative motion breaks a camouflaged target from a same-textured background, thus eliciting discrimination of a motion-defined object. Ring (R) neurons are critical components in the *Drosophila* central complex, which has been implicated in multiple visually guided behaviors. Using two-photon calcium imaging with female flies, we demonstrated that a specific population of R neurons that innervate the superior domain of bulb neuropil, termed superior R neurons, encoded a motion-defined bar with high spatial frequency contents. Upstream superior tuberculo-bulbar (TuBu) neurons transmitted visual signals by releasing acetylcholine within synapses connected with superior R neurons. Blocking TuBu or R neurons impaired tracking performance of the bar, which reveals their importance in motion-defined feature encoding. Additionally, the presentation of a low spatial frequency luminance-defined bar evoked consistent excitation in R neurons of the superior bulb, whereas either excited or inhibited responses were evoked in the inferior bulb. The distinct properties of the responses to the two bar stimuli indicate there is a functional division between the bulb subdomains. Moreover, physiological and behavioral tests with restricted lines suggest that R4d neurons play a vital role in tracking motion-defined bars. We conclude that the central complex receives the motion-defined features via a visual pathway from superior TuBu to R neurons and might encode different visual features via distinct response patterns at the population level, thereby driving visually guided behaviors.

Key words: **central complex; *Drosophila*; motion-defined bar; ring neurons; visual behavior**

Significance Statement

Animals could discriminate a motion-defined object that is indistinguishable with a same-textured background until it moves, but little is known about the underlying neural mechanisms. In this study, we identified that R neurons and their upstream partners, TuBu neurons, innervating the superior bulb of *Drosophila* central brain are involved in the discrimination of high-frequency motion-defined bars. Our study provides new evidence that R neurons receive multiple visual inputs from distinct upstream neurons, indicating a population coding mechanism for the fly central brain to discriminate diverse visual features. These results build progress in unraveling neural substrates for visually guided behaviors.

Introduction

Animals rely on numerous visual signals to navigate through their natural environment and detect their targets. A luminance-defined target is a target defined by its contrast in luminance to the background and has been widely used to investigate the neural mechanisms of motion detection in mammals (Barlow and Levick, 1965; Euler et al., 2002) and invertebrates (Joesch et al., 2010; Mauss et al., 2017). Relative motion is a key feature for detecting a motion-defined target, which has no luminance disparity and is indistinguishable from its surroundings when stationary (Reichardt and Poggio, 1979; Regan and Beverley, 1984). Perception of motion-defined targets is essential for animals to detect camouflaged prey and survive their hidden predators (Stevens and Merilaita, 2009; Stevens and

Received Jan. 23, 2023; revised May 31, 2023; accepted June 2, 2023.

Author contributions: W.D., L.L., and H.W. designed research; W.D., Y.Z., X.Z., J.Y., H.S., and H.W. performed research; W.D., Y.Z., X.Z., and H.W. analyzed data; and W.D. and H.W. wrote the paper.

This study was supported by Natural Science Foundation of China Grants 31871046 to L.L. and 31800867 to H.W. and Strategic Priority Research Program of the Chinese Academy of Sciences Grant XDB37030303. We thank Martin Heisenberg, Reinhard Wolf for technical help in establishing the flight simulator, Haiyun Gong and Xudong Zhao of the Institute of Biophysics Core Facility Center for technical assistance, and Pengbo Hu for codes written in Microsoft Visual Studio.

*W.D., Y.Z., and X.Z. contributed equally to this work.

The authors declare no competing financial interests.

Correspondence should be addressed to Hongying Wei at weihongying@ibp.ac.cn or Li Liu at liuli@ibp.ac.cn.

https://doi.org/10.1523/JNEUROSCI.0128-23.2023

Ruxton, 2019); however, the underlying neural mechanisms remain unclear.

Fruit flies provide an ideal model for elucidating the underlying visual circuits. Previous studies have shown that flies can discriminate a target from the background based on relative motion alone (Reichardt and Poggio, 1979). In the *Drosophila* peripheral visual system, the lobula complex and visual projection neurons have been reported to participate in object motion detection (Fenk et al., 2014; Aptekar et al., 2015). Moreover, particular populations of visual projection neurons are excited by motion- or luminance-defined bars only (Städele et al., 2020), suggesting that different neural mechanisms are involved in the encoding of these different stimuli. However, it remains to be elucidated how motion-defined bars are represented in the central visual system and whether different visual features are represented differentially.

In the *Drosophila* central brain, ring (R) neurons arborizing in the ellipsoid body have been implicated in multiple visually guided behaviors, including visual pattern memory (Wang et al., 2008; Pan et al., 2009) and visual place learning (Ofstad et al., 2011; Kuntz et al., 2012). The postsynaptic sites of R neurons, designated the "bulb," can be divided into superior, inferior, and anterior subdomains, based on their anatomic position (Hanesch et al., 1989; Omoto et al., 2018). Each R neuron extends its dendrites to a single bulb microglomerulus in most cases, forming a sub-type-specific innervation pattern (Hulse et al., 2021). Calcium imaging of R neurons has revealed their coding for luminance-defined stimuli, in which the bulb microglomeruli represent visual landmark positions in a retinotopic order (Seelig and Jayaraman, 2013). The response characteristics of R neurons are thought to be inherited from their upstream inputs, tuberculo-bulbar (TuBu) neurons, which originate in the anterior optic tubercle (AOTU; Omoto et al., 2017; Sun et al., 2017). Recent studies have shown that the visual pathway from TuBu to R neurons also convey signals for polarized light (Hardcastle et al., 2021). These findings strongly suggest that R neurons, receiving inputs from TuBu neurons, are the entry points for visual signals relayed to the central complex.

Here, we investigated the representation of a motion-defined bar in the *Drosophila* central brain. Using two-photon calcium imaging, we identified that a group of superior microglomeruli —innervated by both R and TuBu subpopulations—were activated by a high-frequency motion-defined bar. The blocking of cholinergic signal transmission from TuBu neurons eliminated calcium transients in R neurons and impaired the tracking behavior of a motion-defined bar. These results demonstrate that a motion-defined bar is represented by the central complex via a specific visual pathway from the superior TuBu ($TuBu_s$) neurons to R neurons. Additionally, we observed that most superior R neurons were excited by a low-frequency luminance-defined bar, whereas inferior R neurons displayed two distinct response patterns—excited or inhibited—further indicating the structural and functional division of R subtypes. Our findings provide insight into the neural substrates of visual behavior and highlight the critical functional role of the central complex in multiple feature encoding.

Materials and Methods

Fly stocks. Flies were raised on a standard medium of cornmeal at 25°C under a 12 h light/dark cycle. Three- to seven-day-old female adult flies were used in all experiments. The following fly stocks were used: wild-type Canton S; R20A02-GAL4 (RRID:BDSC_48870); R20A02-LexA (RRID:BDSC_52554); R48B06-GAL4 (RRID:BDSC_50349); c232-GAL4 (a gift from Martin Heisenberg); UAS-mCD8::GFP (RRID:BDSC_5137); UAS-syt::GFP (Zhang et al., 2002); UAS-Dα7::GFP (Leiss et al., 2009); LexAop-mCD8::RFP; LexAop2-post-t-GRASP, UAS-pre-t-GRASP (RRID:BDSC_79040); UAS-GCaMP6s (RRID: BDSC_42746); LexAop-GCaMP6s (RRID:BDSC_44273); UAS-CsChrimson (RRID: BDSC_55134); UAS-nAChRα1 RNAi (THU3068, Tsinghua Fly Center); UAS-nAChRα6 RNAi (RRID:BDSC_52885); UAS-Kir2.1::GFP (RRID: BDSC_6595); UAS-TNTE (RRID:BDSC_28837); Tsh-GAL80 (a gift from Julie Simpson).

Immunochemistry. To examine the expression pattern of driver lines and the GFP Reconstitution Across Synaptic Partners (GRASP) signals, the flies were anesthetized on ice and transferred into PBS. The brains and/or ventral nerve cords (VNCs) were dissected and were then fixed in 4% paraformaldehyde (PFA) for 1–2 h on ice. The samples were then washed for 3× 15 min in PBS containing 0.5% Triton X-100 (PBT) at room temperature and incubated in PBT containing 10% normal goat serum for 1 h at 4°C. Next, the samples were stained with primary and secondary antibodies for 2 d each at 4°C. Following each antibody incubation, the samples were washed in PBT for 3× 15 min again and finally mounted in VECTASHIELD Fluorescent Mounting Media (catalog #H-1000, Vector Laboratories; RRID:AB_2336789). The brain and VNC from the same fly were mounted together.

To examine distribution of choline acetyltransferase (ChAT), we used a modified protocol of Ji et al. (2020). Briefly, the brain samples were dissected and fixed in 4% PFA overnight at 4°C. The samples were then washed for 4× 15 min in PBT, incubated in PBT containing 10% normal goat serum for 3 h at room temperature and stained with primary antibodies for 3 d at 4°C. Next, the samples were washed three times for 8 h in PBS, and stained with secondary antibodies for 1 d at 4°C. After being washed in PBS overnight, the samples were mounted.

Primary antibodies used were mouse anti-Bruchpilot [1:200; catalog #nc82, Developmental Studies Hybridoma Bank (DSHB); RRID:AB_2314866] and mouse anti-ChAT4B1 (1:10; catalog #chat4b1, DSHB; RRID:AB_528122). Secondary antibodies used were Cy3-conjugated goat anti-mouse (1:400; catalog #115-165-062, Jackson ImmunoResearch Labs; RRID:AB_2338685) and goat anti-mouse Alexa Fluor 647 (1:400; catalog #ab150115, Abcam; RRID:AB_2687948). Images were acquired using Zeiss LSM 880 with Airyscan Microscope (RRID:SCR_015963) equipped with 10×, 20×, or 63× objectives and processed with Fiji software (ImageJ; RRID:SCR_002285). We scanned the intact bulb neuropil (see Fig. 4*E*,*F*) and manually counted the number of the microglomeruli that innervated by R (magenta) or/and TuBu (green) neurons using ImageJ, respectively. The proportion of colocalization was calculated via dividing the number of the overlapping microglomeruli by that of R-innervated microglomeruli.

Visual stimuli. For the *in vivo* calcium imaging, the visual stimuli were presented with a curved blue LED display consisting of 128 × 64 pixels. With flies being placed 5 cm above the center of display, the display subtended approximately the visual angle of 128° in the horizontal azimuth and 64° in the vertical elevation. Each pixel subtended 1° at the visual equator. Visual stimuli were generated by custom MATLAB (RRID:SCR_001622) codes and controlled by NovaStudio (Novastar). In most experiments, we used two types of stimuli that we refer to as a motion-defined bar and a luminance-defined bar. A motion-defined bar was composed of a 30° × 64° random-dot based bar moving on a same-textured static background. To reduce onset artifacts, 20 s static background was presented before and after the motion onset. A luminance-defined bar was composed of a 30° × 64° white bar moving on a black background. The motion-defined bar physically contains higher spatial frequency contents than the luminance-defined one. To determine that the calcium responses of superior R neurons to the motion-defined bar were independent on a specific pattern or the switching of individual pixel luminance within the bar, five motion-defined bars with different random dot patterns but the same size (30° × 64°) and shape were used. Stimuli above were presented at a velocity of 40°/s. To further determine the insensitivity of inferior R neurons to the motion-defined bar, moving bars of varying width (4°, 8°, 16°, 48°, and 64°; velocity, 40°/s) and varying moving velocity (20°/s, 40°/s, 60°/s, 80°/s, and 100°/s; width, 30°)

were presented. To test the size tuning properties of superior R neurons in response to the motion-defined bar, moving bars of varying width (4°, 8°, 16°, 30°, 48°, 64°, and 128°; velocity, 40°/s) were presented. Receptive fields were mapped using a 2° white square object presented at a velocity of 20°/s. The square object moved in 32 different elevations at a step of 2°, covering the entire LED display. For all stimuli, the contrast of white and black pixels was 100%. Each stimulus was presented twice, in both directions, from the ipsilateral (ipsi) to contralateral (contra) and from the contra to ipsi side of the recording area. The interval between each stimulus was a 20 s complete darkness.

For the behavior experiments in the flight simulator, the visual stimuli were presented via fiber optics in a panoramic arena consisting of 180 × 32 pixels. With flies being suspended in the center of the arena, the arena subtended the visual angle of 360° in the horizontal azimuth and 90° in the vertical elevation. The motion-defined bar (30° × 90°) based on randomly distributed dots and the luminance-defined ON bar (30° × 90°) were generated and controlled using custom codes written in Visual Studio C# (Microsoft). Each bar started at the center of the arena and oscillated between ±90° at 90°/s. Each stimulus was presented at least three times. At the interval between two stimuli, the flies were provided with a 30° × 90° dark bar in closed loop for 5 s to test whether they noticed the visual stimuli.

In vivo two-photon calcium imaging. Female flies were anesthetized on ice briefly and positioned in a custom holder with a 0.8 × 1.5 mm rounded rectangle hole. The dorsal rim of head capsule was glued to the short side of the hole with UV-curable glue. To minimize the movement of the fly during imaging, additional glue was used around the posterior rim of the head capsule, chest, antenna, and proboscis. In addition, the front legs were removed to prevent occluding vision. Then, the brain was bathed in saline containing the following (in mM): 103 NaCl, 3 KCl, 1.5 $CaCl_2$, 4 $MgCl_2$, 26 $NaHCO_3$, 1 NaH_2PO_4, 10 glucose, 2 sucrose, 10 trehalose, and 5 TES, 2-[Tris(hydroxymethyl)methylamino]-1-ethanesulfonic acid, bubbled with 95% O_2 and 5% CO_2. To expose the recording site, the central dark triangle of the posterior head cuticle and trachea pieces were removed with fine forceps carefully and steadily. Muscle 16 was cut to stop rhythmic movement of the brain if necessary. While recording, the saline was continuously supplied at 1 ml/min.

In the R or TuBu neurons expressing GCaMP6s, the bulb neuropils in the right hemisphere were recorded with 20× objectives (Objective W Plan-Apochromat 20×/1.0 DIC, Zeiss). Three to five image planes were selected to cover the entire bulb, and the distances between adjacent planes were ~6 μm to ensure that different microglomeruli were recorded on each plane. As the brain was immobilized horizontally with the posterior side up, the dorsal and ventral parts of the bulb neuropil were designated the superior bulb and inferior bulb, respectively. Images were acquired at 70.9 Hz (64 × 64 pixels) with 930 nm light. To reduce the phototoxicity, the laser power around the sample position was below 25 mW. At the end of calcium imaging, a stack of high-resolution images (512 × 512 pixels) covering the entire bulb were acquired at high excitation intensity and 0.5 μm step.

Individual microglomerulus was then identified manually as a region of interest (ROI) based on a mean and SD image across the entire time series using ImageJ, with the high-resolution images being taken as a reference to increase the accuracy of ROI selection. The averaging fluorescence intensities within each ROI and the background were computed for each frame via ImageJ, and then further analyses were performed using custom MATLAB codes. For each ROI, the raw response trace (F) was calculated by subtracting the background signal from the averaging fluorescence intensities. ΔF/F0 was calculated by dividing the fluorescence change (ΔF = F–F0) by the mean intensity over 1 s before the stimulus onset (F0). Calcium signals from each trial were then smoothed applying a moving-average filter with a window size of 20. For each stimulus, two repeated trials were averaged to acquire the mean response of a single microglomerulus. Peak ΔF/F0 was defined as the maximum value of the mean response. Because stimulus-independent calcium fluctuations were occasionally observed in the bulb microglomeruli, we have applied the following criteria to distinguish a visually responsive cell: (1) The visual responses to a particular stimulus were consistent across two repeated trials, and (2) the amplitude for an excitatory response was larger than 0.15 ΔF/F0 or the amplitude for an inhibitory response was larger than 0.1 ΔF/F0. Otherwise, ROIs would be considered a nonresponsive group or were excluded from further analysis.

To map the receptive field of a single microglomerulus, at each elevation, we combined the response to a 2° square object moving from the ipsi-to-contra side with those in the opposite direction, and the resulted response trace was downsampled with the spatial resolution of 2°. Then, a 64 × 32 matrix was generated and smoothed using a Gaussian filter. To characterize the excitatory center of the receptive field, its properties including the area, major and minor axis length, eccentricity, and orientation were measured. Only fields with responses larger than 25% of the maximum were calculated.

Optogenetic experiments. Female flies were raised in darkness with standard food containing 0.2 mM all trans-retinal after eclosion for 5–7 d before experiments. To avoid the spurious activation of CsChrimson, the flies were dissected as in immunochemistry but under minimal illumination. The brain sample was immobilized with anterior side up on a poly-D-lysine–coated coverslip and continuously perfused in the same saline as in *in vivo* calcium imaging.

CsChrimson was activated by 595 nm LED light pulses for 20 s. The LED was controlled by custom codes written in Visual Studio C# and delivered at 0.5 Hz. To examine the influence of light intensity on the responses of R neurons, the following light intensities ($\mu W/mm^2$) were used: 0.04, 0.38, 0.91, 1.34, 1.83, 3.06, and 3.91, from low to high. For experiments involving pharmacology, an excitation light at 1.83 $\mu W/mm^2$ was used. The light intensities were measured at the sample position using a power meter (PM100D, Thorlabs). For each light condition, more than three repetitions were tested in experiments. In the control group without expressing CsChrimson, the preparation was perfused with 20 mM KCl for 1 min to test its excitability. R neurons of the right bulb were recorded *ex vivo* via a two-photon microscope with a 20× water-immersion objective. Images were acquired at 15 Hz (128 × 128 pixels) with 930 nm light during experiments. High-resolution image stacks (512 × 512 pixels) covering the entire bulb were acquired at the end of experiments.

Acquired images were processed as in *in vivo* calcium imaging with minor modifications. Briefly, the entire superior region from each brain was recorded as an individual ROI, and the averaged signal within each ROI was measured using ImageJ. For each ROI, ΔF/F0 was calculated by dividing the fluorescence change (ΔF = F–F0) by the mean intensity over 20 s before the stimulus onset (F0). Peak ΔF/F0 was defined as the maximum value of the filtered averaging trace. To characterize the calcium responses at varying illumination conditions, the normalized peak ΔF/F0 was calculated and plotted as a function of light intensity. The recorded cells showed increased response amplitude as the light intensity increased (see Fig. 4*I*). When the light intensity reached 3.06 $\mu W/mm^2$, the saturated responses were observed. For each light condition, the normalized peak ΔF/F0 was defined as the peak ΔF/F0 normalized by that of the saturated response. The relationship between the normalized peak ΔF/F0 and light intensity was modeled by a four-parameter logistic equation using GraphPad Prism 6 (RRID:SCR_002798) software.

Pharmacology. To examine the neural responses to acetylcholine (ACh), the brain preparation was perfused with Ringer solution containing 1 mM ACh for 2 min. To block the cholinergic transmission, Mecamylamine (Meca; antagonist of nicotinic acetylcholine receptors, Sigma-Aldrich) or Scopolamine (Scop, antagonist of metabotropic acetylcholine receptors, MedChemExpress) was added to a final concentration of 50 μM to the sample for 10 min, followed by washing the sample with the drug-free saline. Before, during the drug application, and throughout the wash period, the visual stimuli were presented for the *in vivo* calcium imaging, and the excitation light pulses were given for the *ex vivo* calcium imaging.

Behavioral test. Female flies were cold anesthetized briefly and attached to copper wires by applying a droplet of UV-curable glue between the head and thorax. Before the experiment, the flies were transferred into a chamber containing sugar to acclimate overnight at 25°C. In the flight simulator, the rigid-tethered fly was suspended to a torque meter via a clamp in the center of an optical fiber screen. The torque meter measured the yaw torque signal, which is generated by the steering

effort of flies in the yaw axis, and converted the signal into electrical voltage that was recorded in real time by a data acquisition device (USB-1208FS, Measurement Computing). A positive voltage represented a clockwise turn, and a negative voltage represented a counterclockwise turn. Acquired data were stored on the computer with a sampling rate of 20 Hz using custom Visual Studio C# codes.

The following analyses were performed using custom MATLAB codes. For the open-loop trials, two or three repeated trials for each stimulus were averaged to obtain a mean tracking response of a single fly. To evaluate the tracking performance of flies, we calculated the correlations between their steering trajectories and stimulus positions. To quantify the variability in steering trajectories within each fly group, traces were normalized by performing a *z*-score transformation, and then SDs were calculated for the entire duration of the stimulus presentation. For the closed-loop phase, the position of a black bar was controlled by the tethered fly. The flies that could not frontally fixate the dark bar or stopped during experiments were excluded in our analysis.

Experimental design and statistical analysis. For *in vivo* two-photon calcium imaging that is used to analyze the calcium responses of R or TuBu neurons to both the luminance- and motion-defined bars, 116 ROIs from 10 flies were selected for testing the calcium responses of R neurons labeled by R20A02-GAL4, 64 ROIs from 7 flies for TuBu neurons labeled by R48B06-GAL4, and 84 ROIs from 7 flies for R4d neurons labeled by c232-GAL4. To compare the calcium responses of superior R neurons to motion-defined bars with five different random dot patterns, 10 ROIs from 6 flies were selected. To compare the calcium responses of superior R neurons to motion-defined bars of varying width, 10 ROIs from 6 flies were selected. In pharmacology experiments, six flies (*in vivo*) or brain samples (*ex vivo*) were used to identify the neurotransmitter for TuBu to R neuronal signaling. For all experiments above, peak calcium responses of ROIs were compared between two or more groups. A two-tailed paired *t* test was used to compare two groups if the normal distribution could be assumed; otherwise Wilcoxon matched-pairs signed-rank test was used. Repeated-measures ANOVA (Friedman test) was used to compare five groups that presented with different motion-defined bars as the data were not normally distributed.

For RNAi experiments, 10 ROIs from 5 flies were selected in the control group, and 9 ROIs from 5 flies were selected in two experimental groups. For optogenetic experiments with excitation light at 1.83 μW/mm^2, 6 and 10 brain samples were examined in control and experimental groups, respectively. For these experiments, an unpaired *t* test was performed to compare the peak calcium responses between two groups if the normal distribution could be assumed, otherwise a Mann–Whitney test was performed.

For behavioral experiments, 14–18 flies were examined in two parental control and experimental groups. The detailed sample size of each group can be found in the figure legends. The correlations and SDs were compared among three groups. If the data were normally distributed, one-way ANOVA with Tukey's multiple comparisons was performed when variances were equal; otherwise, the Brown–Forsythe ANOVA with Tamhane's test was used. If the data were not normally distributed, the Kruskal–Wallis test with Dunn's test was performed.

Statistical analysis was conducted using GraphPad Prism 6 or IBM SPSS 23.0 (RRID:SCR_002865) statistical software. Shapiro–Wilk normality tests were performed to test whether data were normally distributed. The statistical significance of tests was indicated as $^{***}p < 0.001$, $^{**}p < 0.01$, $^{*}p < 0.05$, and (n.s.) $p > 0.05$.

Code availability. Custom codes used in this study are available from the corresponding author on reasonable request.

Results

Bulb microglomeruli of R neurons show distinct response patterns to motion- and luminance-defined bars

To examine whether R neurons are involved in the encoding of motion-defined bars and whether the encoding of motion- and luminance-defined bars differed in their signal transduction pathways, we analyzed the visual responses of bulb microglomeruli, focusing on the superior and inferior subdomains, which are spatially distinct. R20A02-GAL4 was used as the driver because this line labels most R neurons (Fig. 1*A*,*B*), including R2, R3w, R4d, and R5 microglomeruli in the superior bulb and R3d/m/p microglomeruli in the inferior bulb, according to a previous study using the MultiColor FlpOut technique (Fisher et al., 2019). A 30° × 64° motion- or luminance-defined bar moved at 40°/s on a curved LED screen placed in front of flies, and two-photon calcium imaging was conducted to record calcium signals *in vivo* (Fig. 1*C*,*D*). With the expression of the genetically encoded indicator GCaMP6s, three to five image planes were selected to cover all detectable microglomeruli in each hemisphere.

In the superior bulb, we observed that a group of microglomeruli, named superior R group 1, responded robustly to both motion- and luminance-defined bars, whether the bar was moving from the ipsilateral to contralateral side of the recorded bulb or in the opposite direction (Fig. 1*E*,*F*,*I*,*J*, green; 19 ROIs in 10 flies). A part of the remaining microglomeruli in the superior bulb, named superior R group 2, were excited by a luminance-defined bar only (Fig. 1*G*–*J*, orange; 44 ROIs in 10 flies). The motion-defined bar induced significantly smaller calcium increases than the luminance-defined bar in the superior R group 1 neurons (Fig. 1*K*). In the inferior bulb, we did not observe any responses to a motion-defined bar, whereas a luminance-defined bar induced variable responses. We observed calcium increases in a subset of microglomeruli, named inferior R group 1 (Fig. 1*L*,*M*,*P*,*Q*, pink; 6 ROIs in 10 flies), and calcium decreases in another subset of microglomeruli, named inferior R group 2 (Fig. 1*N*–*Q*, blue; 5 ROIs in 10 flies). The inferior R neurons were insensitive to motion-defined bars of varying width (Fig. 1*R*; 4°, 8°, 16°, 48° and 64°) or moving velocity (Fig. 1*S*; 20°/s, 40°/s, 60°/s, 80°/s and 100°/s). In addition, some microglomeruli were unresponsive to any of our stimuli (Fig. 1*I*,*J*,*P*,*Q*, gray; 5 ROIs in the superior bulb and 37 ROIs in the inferior bulb from 10 flies).

Together, our results indicate that motion- and luminance-defined bars are encoded by different response patterns of spatially segregated bulb microglomeruli of R neurons. Specifically, both superior and inferior R neurons are involved in the signal transduction of a luminance-defined bar, whereas only a specific group of superior R neurons respond to a motion-defined bar. Notably, the microglomeruli in this group were preferentially located within the dorsolateral part of the superior bulb (Fig. 1*E*), where the dendrites of R4d neurons are reported to innervate (Hulse et al., 2021).

Superior R neurons respond to high-frequency motion-defined bars with pattern-independent and size-tuning properties

We further investigated the visual response properties of the superior R group 1 neurons. Responsive microglomeruli were stimulated by five motion-defined bars with different random dot patterns (Fig. 2*A*). There were no significant differences between calcium responses of the same microglomerulus to the five stimulations, suggesting a general encoding mechanism for motion-defined bars. Responses induced by five motion-defined bars were not direction selective (Fig. 2*B*). Moreover, the receptive fields of responsive neurons were mapped using a 2° ON square that moved horizontally. Superior R group 1 neurons had receptive fields that covered a large part of the ipsilateral visual field near the midline of the display, much larger than the spatial extent of the luminance gaps contained within the motion-defined bar stimuli (Fig. 2*C*; major axis, 35.6° ± 3.6°; minor axis,

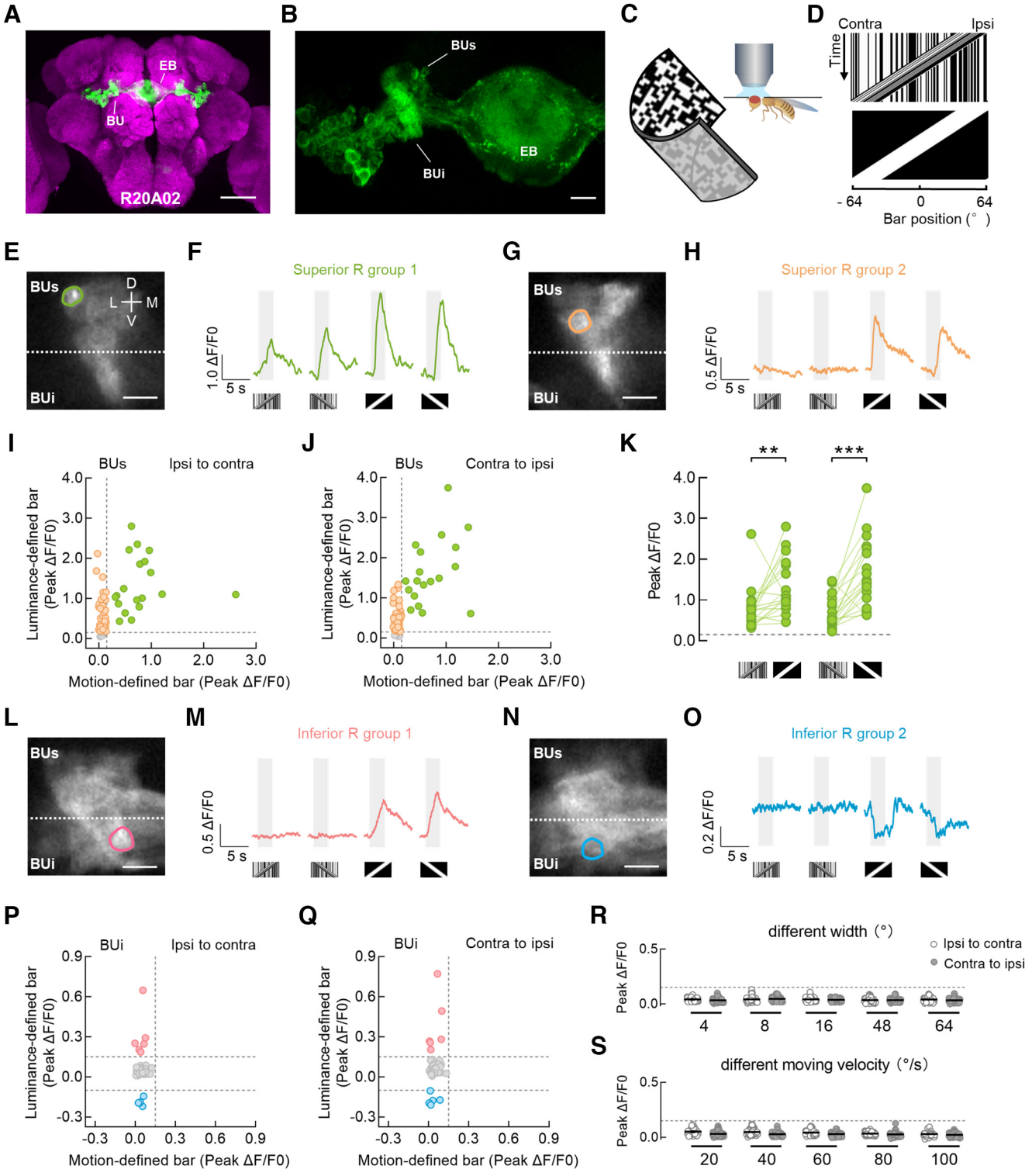

Figure 1. Bulb microglomeruli of ring neurons respond distinctly to different bar stimuli. ***A***, Anatomy of R neurons labeled by R20A02-GAL4 driving the expression of UAS-mCD8::GFP (green) in the central brain. Neuropil was immunostained with anti-Bruchpilot (magenta). EB, ellipsoid body; BU, bulb. Scale bar, 100 μm. ***B***, The drive line in ***A*** targeted most of the R neurons (green) innervating the superior bulb (BUs) and inferior bulb (BUi). Scale bar, 10 μm. ***C***, Setup for the two-photon *in vivo* calcium imaging experiments. ***D***, Space–time plots for a 30° × 64° motion-defined bar (top) and a 30° × 64° luminance-defined bar (bottom) that were moving at 40°/s from the Ipsi to the Contra side of the right bulb. These bars are used in ***E***–***Q***. ***E***, ***F***, Two-photon excitation image (***E***) and calcium responses (***F***) of an example microglomerulus in the superior bulb. The superior and inferior neuropils are classified as the top and bottom regions, respectively, divided by the dotted line (***E***). The example cell exhibited excitation to both motion- and luminance-defined bars. This cell type is referred to as the superior R group 1. Visual stimuli were presented in both horizontal directions. For each stimulus, response from a single trial is shown in ***F***. The gray-shaded regions represent duration of stimulation (2.5 s). D, Dorsal; V, ventral; M, medial; L, lateral. ***G***, ***H***, Two-photon excitation image (***G***) and calcium responses (***H***) of another example microglomerulus in the superior bulb. The example cell did not respond to motion-defined bars but was excited by luminance-defined bars. This cell type is referred to as the superior R group 2. ***I***, ***J***, Peak calcium responses from all recorded superior R neurons to ipsi-to-contra motion (***I***) and contra-to-ipsi motion (***J***). Each dot represents a single microglomerulus. ROIs with the same color showed homogeneous visual responses. Superior R group 1 neurons are indicated as green dots; $n = 19$ ROIs in 10 flies. Superior R group 2 neurons are indicated as orange dots; $n = 44$ ROIs in 10 flies. Microglomeruli that did not respond to any of our stimuli are

25.4° ± 3.1°). A 30° × 64° motion-defined bar almost fits the widths of the receptive fields of superior R group 1 neurons (Fig. 2*D*), which contains high spatial frequency features. We next recorded neural responses to motion-defined bars of varying width. The superior R group 1 neurons were sensitive to bars of all tested sizes (Fig. 2*E*; 4°, 8°, 16°, 30°, 48°, 64°, and 128°). When the bar was narrower (16° or less) than their receptive fields, the response amplitudes of superior R group 1 neurons were significantly smaller. However, as the bar widened to cover their receptive fields, the response amplitudes statistically increased and saturated (30°), showing a spatial tuning property in the horizontal dimension (Fig. 2*E*,*F*).

In summary, our results indicate that the superior R neurons are actively encoding the high spatial frequency feature of motion-defined bars, rather than a specific patten or the switching of individual pixel luminance within the bar, in a pattern-independent and spatial saturated manner.

$TuBu_s$ neurons respond to a motion-defined bar

As well as the dendrites of R neurons, many neuronal axons are also intermingled in the bulb neuropil, forming complex connection networks (Scheffer et al., 2020; Hulse et al., 2021). One type of potential inputs, TuBu neurons, extend their neurites from AOTU to the bulb (Omoto et al., 2017; Hulse et al., 2021). To determine whether TuBu neurons encode a motion-defined bar, we measured the visual responses of TuBu neurons targeted by the R48B06-GAL4 driver. The driver labels TuBu neurons that project from the lateral and intermediate AOTU to the $TuBu_s$ and inferior TuBu ($TuBu_i$), respectively (Fig. 3*A*). Similar to R neurons, a motion-defined bar evoked excitatory responses in a group of $TuBu_s$ neurons, regardless of the motion direction (Fig. 3*B–F*, green; 27 ROIs in 7 flies). No fluorescence changes during the stimulation period were observed in the remaining $TuBu_s$ or $TuBu_i$ neurons (Fig. 3*B–F*, orange; 12 ROIs in 7 flies; pink, 25 ROIs in 7 flies, respectively). Further, all recorded microglomeruli in the superior and inferior bulbs were excited by a luminance-defined bar (Fig. 3*C–F*). As with the superior R group 1 neurons, $TuBu_s$ neurons showed larger responses to a luminance-defined bar than to a motion-defined one (Fig. 3*G*). The population of $TuBu_s$ neurons that were sensitive to the motion-defined bar sampled a wide part of the ipsilateral visual hemisphere, near the visual midline (Fig. 3*H*; major axis, 41.5° ± 4.3°; minor axis, 19.0° ± 1.8°).

Hence, we identified that a population of $TuBu_s$ neurons responded to a motion-defined bar, which suggests that visual information might be delivered from $TuBu_s$ to superior R neurons and helps to further characterize the different response properties of the bulb subdomains.

Superior R neurons form direct connections with upstream $TuBu_s$ neurons

To test possible synaptic contacts, we examined the locations of presynaptic and postsynaptic markers in both TuBu and R neurons. Immunostaining images showed that TuBu neurons extended presynaptic axons into the bulb neuropil, whereas R neurons projected postsynaptic dendrites (Fig. 4*A–D*), thus indicating a signaling pathway from TuBu to R neurons. Furthermore, dual-color labeling of TuBu and R neurons revealed that their branches overlapped in the expected bulb regions (Fig. 4*E*). To quantify potential synaptic contacts, the colocalization ratio was calculated by dividing the number of the overlapping microglomeruli by that of the microglomeruli belonging to R neurons only. Statistical analysis revealed that ~70% of microglomeruli were innervated by both neuronal populations, both in the superior and inferior bulbs (Fig. 4*F*).

To provide further evidence for synaptic partners, targeted GRASP experiments were performed to confirm that TuBu neurons were upstream of R neurons. The reconstituted GFP signal was detected specifically in the bulb when targeting split-GFP11 to the presynaptic sites of TuBu neurons and split-GFP1-10 to the postsynaptic sites of R neurons (Fig. 4*G*).

To examine functional connectivity in the superior bulb, we performed *ex vivo* calcium imaging combined with optogenetics. In the experimental group, light-activated CsChrimson was expressed in TuBu neurons, and the activity of superior R neurons was recorded via two-photon microscopy. Excitation light with low to high intensity was produced in sequence to artificially activate TuBu neurons so that the magnitude of calcium responses increased monotonically as the light intensity increased. We detected little calcium transients of superior R neurons below 0.38 $\mu W/mm^2$, increasing responses over 0.91 $\mu W/mm^2$, and the maximum response of ~3.06 $\mu W/mm^2$ (Fig. 4*H*). The light-intensity-dependent responses of the experimental group fit the sigmoidal curve well (Fig. 4*I*), thus indicating that TuBu neurons provide excitatory inputs to superior R neurons. In contrast, no light-evoked responses were observed in the control flies (without expression of CsChrimson), although selected microglomeruli were activated by Ringer solution containing 20 mM KCl (Fig. 4*J*). In the following optogenetic experiments involving pharmacology, an excitation light of 1.83 $\mu W/mm^2$ was used for a better signal-to-noise ratio. With this excitation, the peak fluorescence changes of the experimental group were significantly greater than those of the control group (Fig. 4*K*).

Together, our results indicate there are direct structural and functional connections between R and TuBu neurons, which provides an anatomic and physiological basis to suggest that superior R neurons receive synaptic inputs from $TuBu_s$ neurons.

nAChR-mediated visual pathway from $TuBu_s$ to superior R neurons encodes the motion-defined bar

We next investigated the neurotransmitter system responsible for the signaling from $TuBu_s$ to R neurons. The application of

←

indicated as gray dots (bottom); $n = 5$ ROIs in 10 flies. The horizontal and vertical dotted lines indicate 0.15 ΔF/F0. ***K***, Comparison of peak responses from the superior R group 1 neurons between a motion-defined bar and a luminance-defined bar. Left, stimuli moved from ipsi to contra; Wilcoxon matched-pairs signed-rank test, $W = 142$, $p = 0.0028$. Right, stimuli moved from contra to ipsi; Wilcoxon matched-pairs signed-rank test, $W = 142$, $p = 0.0001$. The horizontal dotted line indicates 0.15 ΔF/F0. ***L***, ***M***, Two-photon excitation image (***L***) and calcium responses (***M***) of an example microglomerulus in the inferior bulb. The example cell was insensitive to motion-defined bars but was activated by luminance-defined bars. This cell type is referred to as the inferior R group 1. ***N***, ***O***, Two-photon excitation image (***N***) and calcium responses (***O***) of another example microglomerulus in the inferior bulb. The example cell did not respond to motion-defined bars but was inhibited by luminance-defined bars. This cell type is referred to as the inferior R group 2. Scale bars: ***E***, ***G***, ***L***, ***N***, 10 μm. ***P***, ***Q***, Peak calcium responses from all recorded inferior R neurons to ipsi-to-contra motion (***P***) and contra-to-ipsi motion (***Q***). Inferior R group 1 neurons are indicated as pink dots; $n = 6$ ROIs in 10 flies. Inferior R group 2 neurons are indicated as blue dots; $n = 5$ ROIs in 10 flies. Microglomeruli that did not respond to any of our stimuli are indicated as gray dots; $n = 37$ ROIs in 10 flies. The top and bottom horizontal dotted lines indicate 0.15 ΔF/F0 and −0.10 ΔF/F0, respectively. The vertical dotted line indicates 0.15 ΔF/F0. ***R***, Peak calcium responses of inferior R neurons to motion-defined bars of varying bar width (4°, 8°, 16°, 48°, and 64°). Each bar moved at 40°/s in both horizontal directions; $n = 41$ ROIs in 6 flies. The horizontal dotted line indicates 0.15 ΔF/F0. Black lines indicate mean ± SEM across microglomeruli. ***S***, Peak calcium responses of inferior R neurons to a 30° × 64° motion-defined bar moving at 20°—100°/s. Each bar was presented in both horizontal directions; $n = 47$ ROIs in 6 flies. The horizontal dotted line indicates 0.15 ΔF/F0. Black lines indicate mean ± SEM across microglomeruli. ***$p < 0.001$, **$p < 0.01$.

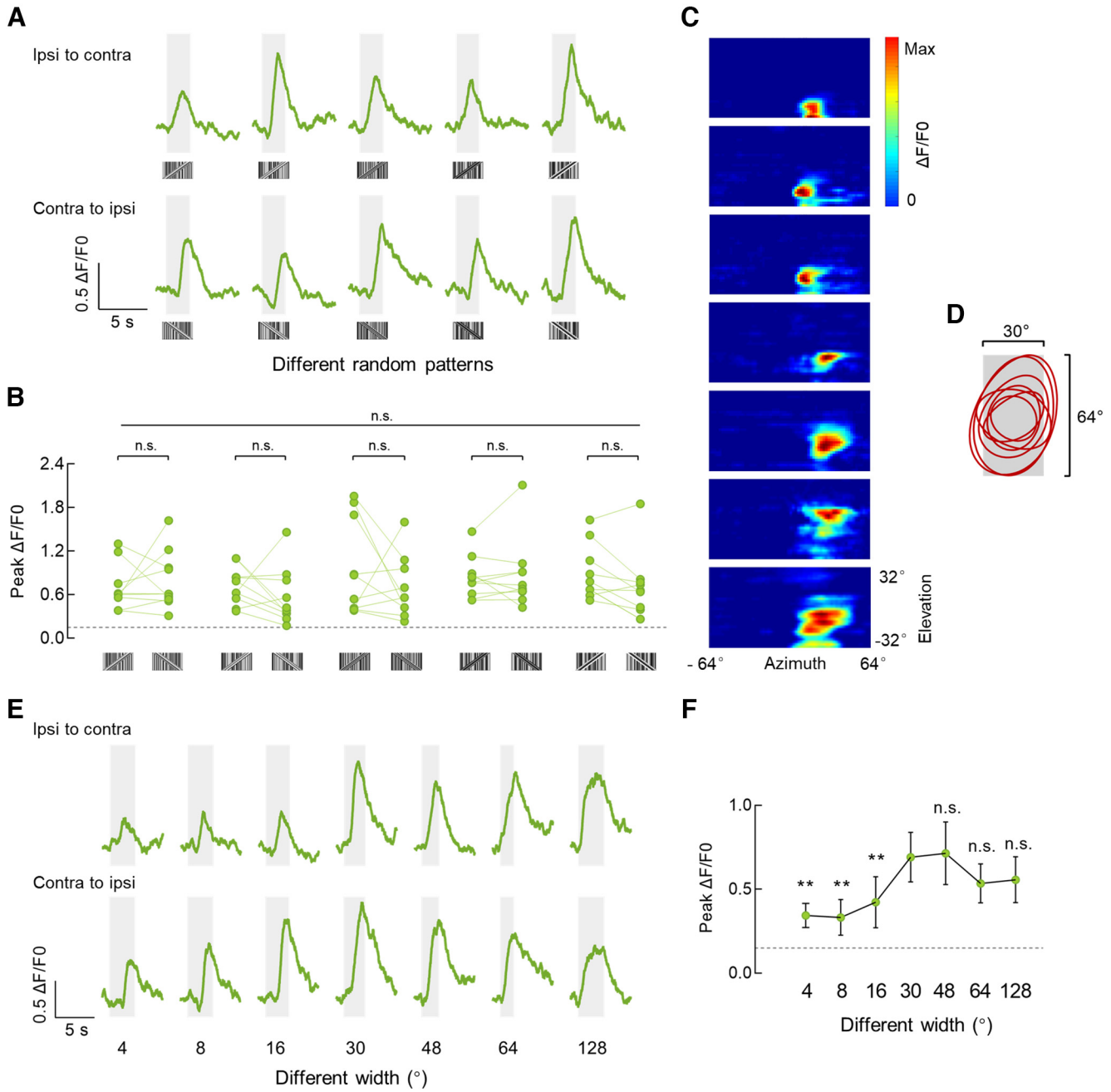

Figure 2. Physiologic properties of the superior R neurons that are sensitive to motion-defined bars. ***A***, Calcium responses of an example superior R neuron to 30° × 64° motion-defined bars with five different random patterns. Stimuli were presented in both horizontal directions at 40°/s. The gray-shaded regions represent duration of stimulation (2.5 s). ***B***, Comparison of peak responses from all recorded microglomeruli ($n = 10$ ROIs from 6 flies) to motion-defined bars with five different random patterns. Repeated-measures ANOVA (Friedman test) was used to compare all five groups (top, long line), Friedman's $F = 17.56$, n.s., $p = 0.0923$. For each pattern, peak responses to the bar moving in two horizontal directions were compared (bottom, short lines). Two-tailed paired t test was used for the fourth pattern, and Wilcoxon matched-pairs signed-rank test was used for other patterns. From the first to the fifth pattern, $W = 7$, $p = 0.7695$; $W = 25$, $p = 0.2324$; $W = 19$, $p = 0.3750$; $t_{(9)} = 2.076$, $p = 0.0677$; $W = 37$, $p = 0.0645$. The horizontal dotted line indicates 0.15 ΔF/F0. ***C***, Receptive field maps for microglomeruli of R neurons that were responsive to motion-defined bars; $n = 7$ ROIs in 5 flies. A 2° ON square object moved at 32 different elevations in both directions was used to map the receptive field. ***D***, The contours (25% maximum) of all estimated receptive fields in ***C***. The gray-shaded region indicates a 30° × 64° bar stimulus. ***E***, Calcium responses of an example superior R neuron to motion-defined bars of varying bar width (4°, 8°, 16°, 30°, 48°, 64°, and 128°). Each bar moved at 40°/s in both horizontal directions. ***F***, Peak calcium responses of superior R neurons to motion-defined bars of varying bar width. Peak calcium responses to each bar moving in both directions were averaged; $n = 10$ ROIs in 6 flies. The responses to the 30° bar were compared with those to the bar of other sizes, respectively. All comparisons were analyzed with Wilcoxon matched-pairs signed-rank tests; 30° versus 4/8/16°, $W = 55$, $p = 0.002$; 30° versus 48°, $W = 7$, $p = 0.7695$; 30° versus 64°, $W = 10$, $p = 0.1309$; 30° versus 128°, $W = 10$, $p = 0.2324$. The horizontal dotted line indicates 0.15 ΔF/F0. Error bars indicate SEM. $^{**}p < 0.01$.

1 mM ACh generated intracellular calcium transients in the superior microglomeruli of R neurons (Fig. 5*A*). To test whether TuBu neurons are cholinergic, we examined the expression of ChAT, a critical enzyme for ACh synthesis. The colocalization of transmembrane GFP and anti-ChAT fluorescence in cell bodies indicated that TuBu neurons release ACh (Fig. 5*B–D*).

To determine the role of cholinergic neurotransmission and identify the responsible receptor subtype, we used simultaneous optogenetic and pharmacologic tests in combination with *ex vivo*

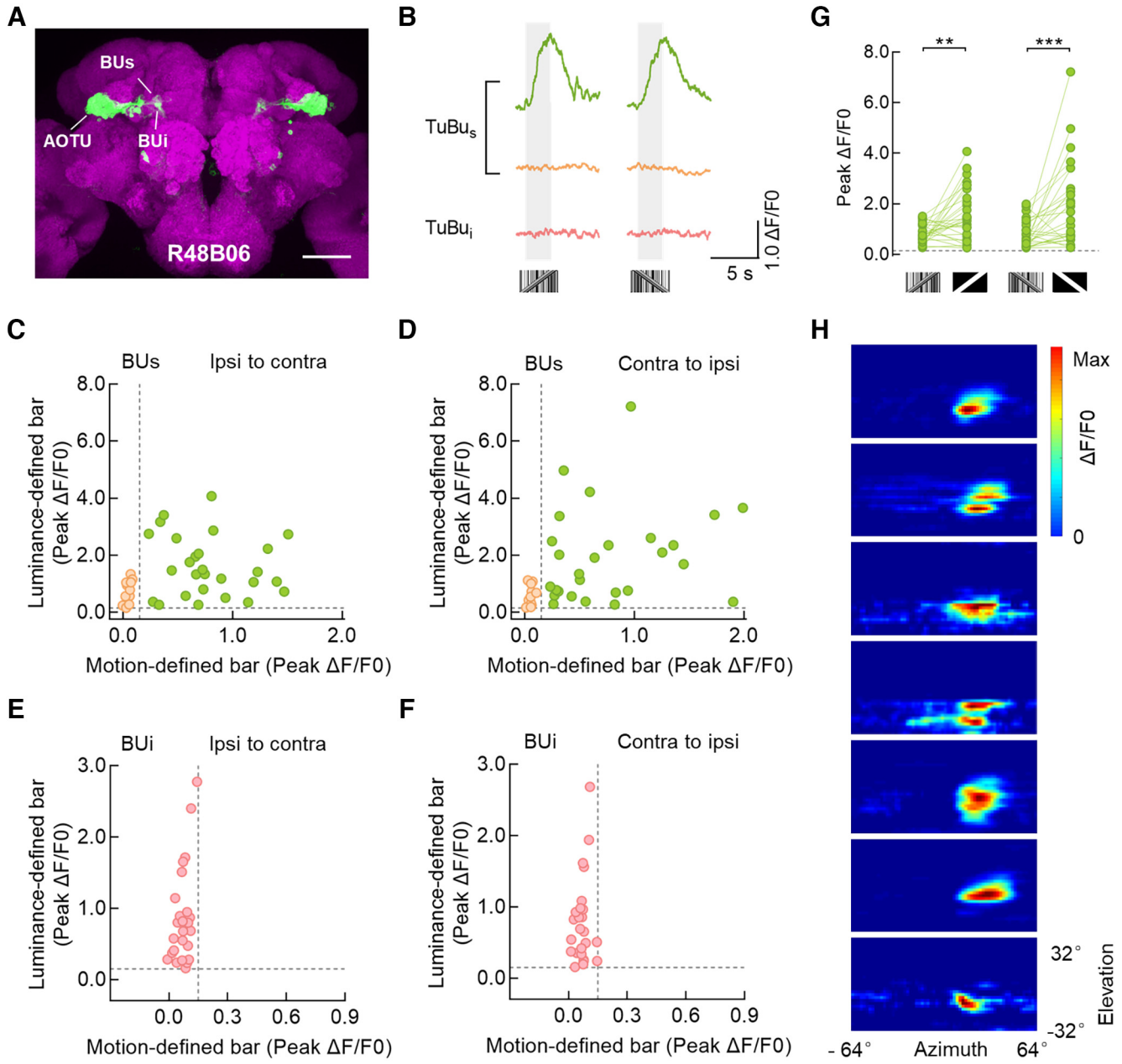

Figure 3. Superior tuberculo-bulbar neurons respond to a motion-defined bar. ***A***, Anatomy of TuBu neurons labeled by R48B06-GAL4 driving the expression of UAS-mCD8::GFP (green). This driver line labeled TuBu neurons that project from the AOTU to the superior bulb (BUs) and inferior bulb (BUi). Neuropil was immunostained with anti-Bruchpilot (magenta). Scale bar, 100 μm. ***B***, Calcium responses of three example microglomeruli of TuBu neurons to a 30° × 64° motion-defined bar moving at 40°/s. An example cell in the superior bulb responded to a motion-defined bar in both directions (green), whereas another example cell in the superior bulb did not (orange). The example cell in the inferior bulb did not respond to motion-defined bars (pink). The gray-shaded regions represent duration of stimulation (2.5 s). ***C***, ***D***, Peak calcium responses from all recorded TuBu$_s$ neurons to a 30° × 64° motion- and luminance-defined bar moving at 40°/s from ipsi to contra (***C***) and contra to ipsi (***D***). Each dot represents a single microglomerulus. ROIs with the same color showed homogeneous visual responses. ROIs that responded to both motion and luminance-defined bars are indicated as green dots; $n = 27$ ROIs in 7 flies. ROIs that responded to luminance-defined bars but not motion-defined bars are indicated as orange dots, $n = 12$ ROIs in 7 flies. The horizontal and vertical dotted lines indicate 0.15 ΔF/F0. ***E***, ***F***, Peak calcium responses from all recorded TuBu$_i$ neurons to a 30° × 64° motion- and luminance-defined bar moving at 40°/s from ipsi to contra (***E***) and contra to ipsi (***F***). ROIs that responded to luminance-defined bars but not motion-defined bars are indicated as pink dots; $n = 25$ ROIs in 7 flies. The horizontal and vertical dotted lines indicate 0.15 ΔF/F0. ***G***, Comparison of peak responses from the recorded TuBu$_s$ neurons, green dots in ***C*** and ***D***, between a motion- and luminance-defined bar. Left, Stimuli moved from ipsi to contra, two-tailed paired t test, $t_{(26)} = 3.704$, $p = 0.001$. Right, Stimuli moved from contra to ipsi; Wilcoxon matched-pairs signed-rank test, $W = 298$, $p = 0.0001$. The horizontal dotted line indicates 0.15 ΔF/F0. ***H***, Receptive field maps for microglomeruli of TuBu$_s$ neurons that were responsive to motion-defined bars; $n = 7$ ROIs in 6 flies. ***$p < 0.001$, **$p < 0.01$.

calcium imaging (Fig. 5*E*). We optically activated TuBu neurons in the presence of ACh receptor blockers. Preincubation with the nicotinic ACh receptor (nAChR) antagonist Meca (50 μM) for 10 min blocked the light-induced responses of superior R neurons (Fig. 5*F*,*G*), whereas the muscarinic antagonist Scop (50 μM) did not (Fig. 5*H*,*I*). Washout of the drugs with Ringer solution resulted in the sufficient recovery of calcium levels (Fig. 5*F–I*).

To further characterize the contribution of ACh in the signal transduction of a motion-defined bar, the visual responses of superior R neurons were imaged *in vivo* with exposure to ACh receptor blockers (Fig. 5*J*). Before the

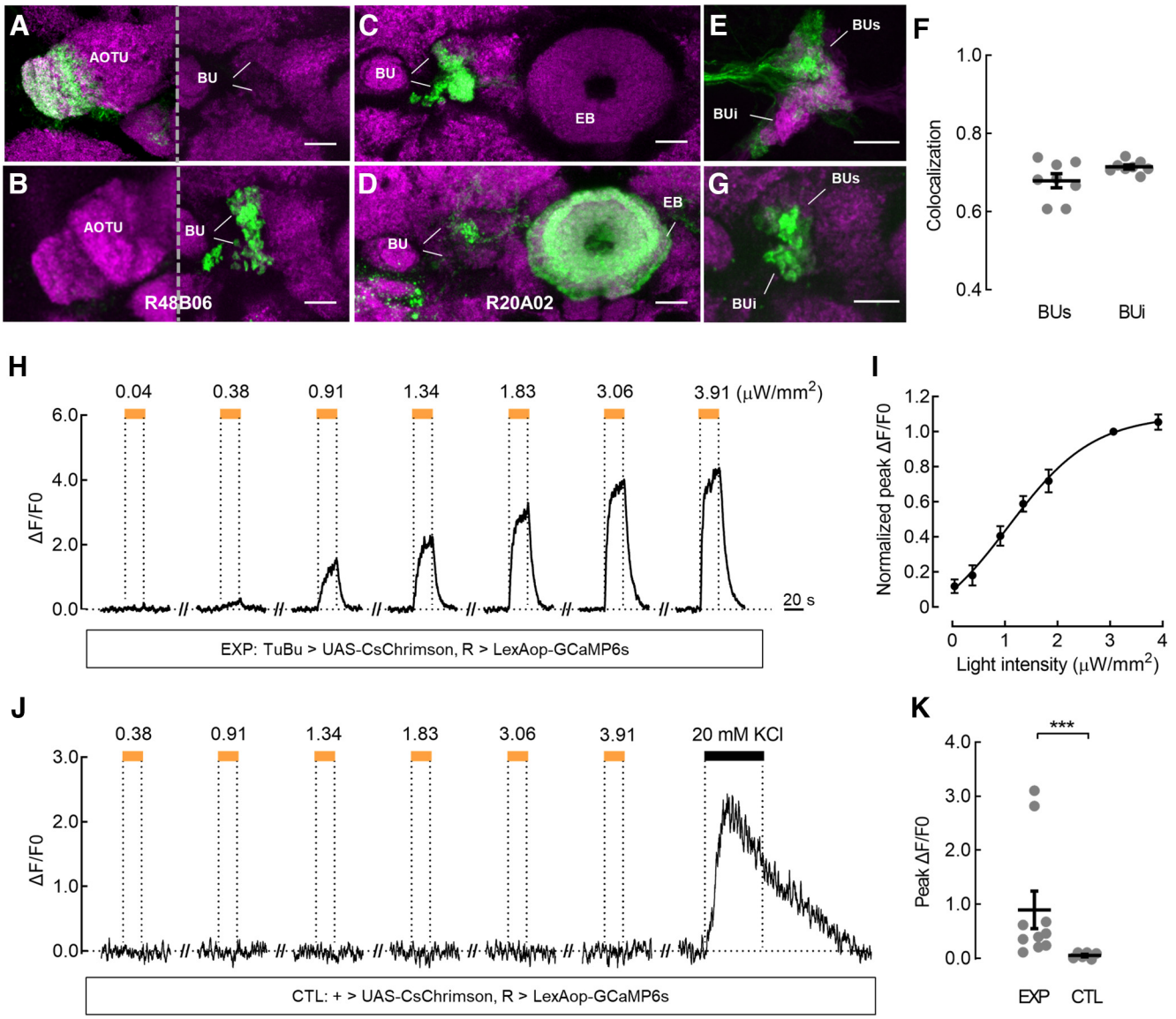

Figure 4. Superior ring neurons receive direct inputs from superior tuberculo-bulbar neurons. ***A***, ***B***, Expression of the postsynaptic marker Dα7::GFP (***A***) and presynaptic marker Syt::GFP (***B***) in TuBu neurons labeled by R48B06-GAL4. ***C***, ***D***, Expression of the postsynaptic marker Dα7::GFP (***C***) and presynaptic marker Syt::GFP (***D***) in R neurons labeled by R20A02-GAL4. Neuropil was immunostained with anti-Bruchpilot (***A–D***, magenta). ***E***, ***F***, TuBu neurons (green) were labeled with UAS-CD8::GFP using R48B06-GAL4, and R neurons (magenta) were labeled with LexAop-CD8::GFP using R20A02-LexA. Overlap was observed in the superior bulb (BUs) and inferior bulb (BUi) subdomains (***E***). Overlapping microglomeruli were nearly 70% of all the detected superior and inferior microglomeruli of R neurons (***F***); $n = 8$ hemispheres. Black lines indicate mean ± SEM across hemispheres. ***G***, TuBu neurons expressed pre-t-GRASP and R neurons expressed post-t-GRASP using the same driver lines as ***E***. GRASP signal was observed in both superior and inferior bulbs. Neuropil was immunostained with anti-Bruchpilot (magenta). Scale bars: ***A–G***, 10 μm. ***H***, *Ex vivo* calcium responses of R neurons when CsChrimson was expressed in TuBu neurons in the experimental group (EXP). The same driver lines were used as in ***E***. The superior bulb neuropil of R neurons in the right hemisphere was recorded as an individual ROI. The responses to 595 nm light pulses of the indicated powers are shown. Light pulses at intensities higher than 0.38 μW/mm^2 triggered a robust calcium influx. Excitatory responses reached a maximum level near 3.06 μW/mm^2. The horizontal orange bars represent the light stimulation period (20 s). ***I***, The normalized peak responses of R neurons exhibited light intensity-dependent increases in EXP; $EC_{50} = 1.06$ μW/mm^2; $n = 10$ flies. Error bars indicate SEM. ***J***, Calcium responses of R neurons without CsChrimson expression in the control group (CTL). No fluorescence changes were observed with the application of light pulses, although an immediate fluorescence increase was evoked by Ringer solution containing 20 mM KCl (black horizontal bar). ***K***, Comparison of peak responses between EXP and CTL. The light power was 1.83 μW/mm^2. For the EXP group, $n = 10$ flies. For the CTL group, $n = 6$ flies; Mann–Whitney test, $U = 0$, $p = 0.0002$. Black lines indicate mean ± SEM across flies. ***$p < 0.001$.

drug application, R neurons responded robustly to the bar stimuli. However, in the presence of 50 μM Meca, visually evoked responses were abolished and then partially recovered following washout (Fig. 5*K*,*L*). In contrast, 50 μM Scop had no significant effects on the response amplitude of R neurons (Fig. 5*M*,*N*). Furthermore, we observed that the RNAi-mediated knockdown of nAChR subunit Dα1 or Dα6 in R neurons significantly reduced their visual responses to the motion-defined bar compared with the control group (Fig. 5*O*,*P*).

Thus, the results of our pharmacological investigation and RNAi experiments indicate that ACh is responsible for relaying motion-defined visual information, possibly from $TuBu_s$ neurons to superior R neurons via nAChR.

Normal tracking behavior to a motion-defined bar requires the TuBu–R pathway

Flies actively steer toward a luminance- or motion-defined bar (Theobald et al., 2010; Bahl et al., 2013), which motivated our investigation into the function of R and TuBu neurons in bar

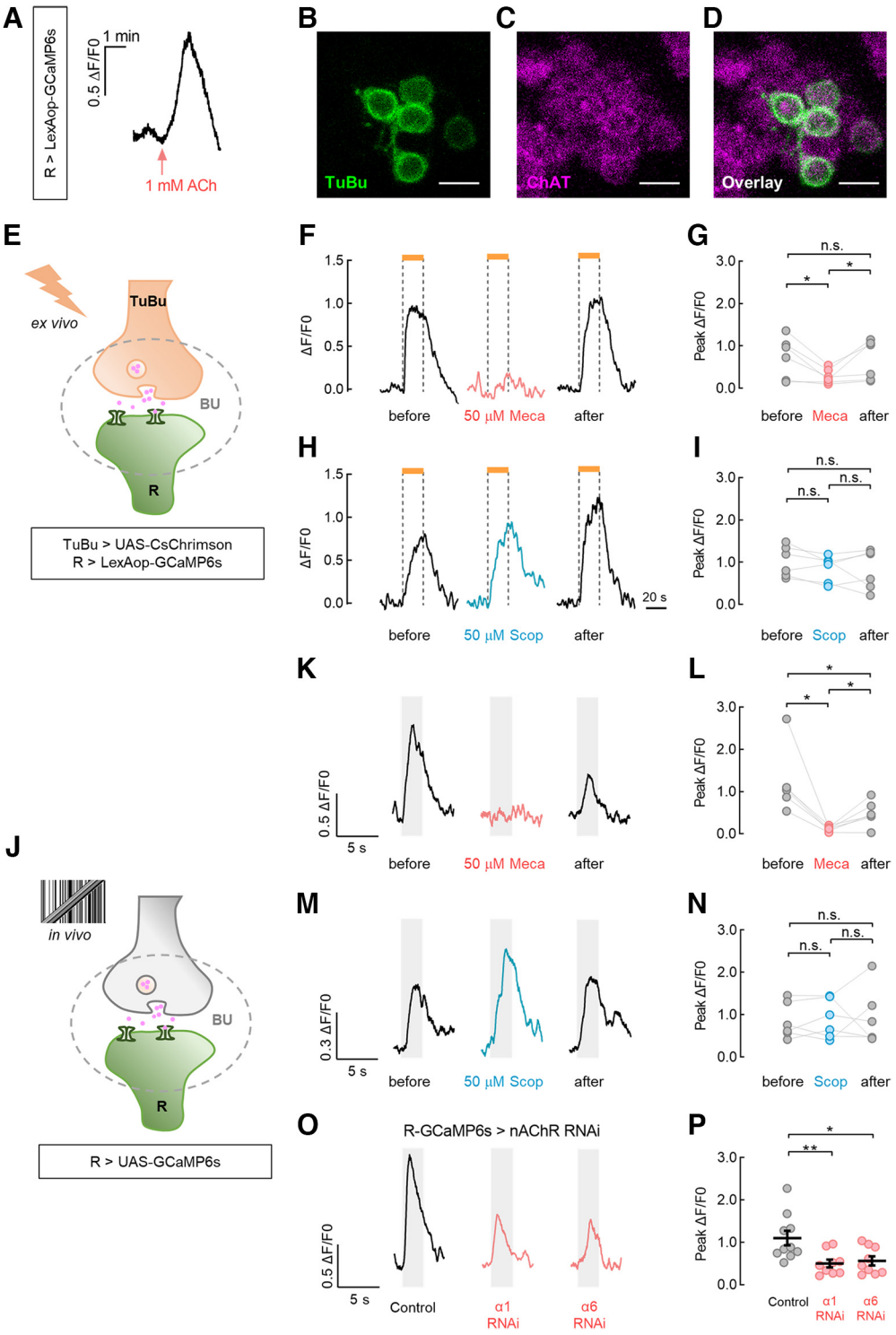

Figure 5. Nicotinic ACh receptor is required for ring neurons to receive visual signals from tuberculo-bulbar neurons. ***A***, Application of 1 mM ACh induced an intracellular calcium increase in R neurons. ***B–D***, TuBu neurons expressing UAS-mCD8::GFP (***B***, green) were immunostained with anti-ChAT (***C***, magenta). Colocalization of anti-ChAT and GFP signals are shown (***D***, overlay). Scale bars, 5 μm. ***E***, Schematic diagram of the *ex vivo* calcium imaging experiments combined with optogenetics and pharmacology. ***F–I***, Optogenetic activation of TuBu neurons triggered calcium increases in R neurons that were blocked by preincubation with Meca (***F***, 50 μM) for 10 min, but not by Scop (***H***, 50 μM). The horizontal orange bars represent the light stimulation period (20 s). The results of the statistical analysis were as indicated (***G*** and ***I***). For Meca treatment, $n = 6$ flies. Before versus Meca, two-tailed paired t test, $t_{(5)} = 3.259$, $p = 0.0225$; Meca versus after, Wilcoxon matched-pairs signed-rank test, $W = 21$, $p = 0.0313$. Before versus after, Wilcoxon matched-pairs signed-rank test, n.s., $W = 3$, $p = 0.8438$. For Scop treatment, $n = 6$ flies. Two-tailed paired t tests were used in all comparisons. Before versus Scop, $t_{(5)} = 2.054$, $p = 0.0952$; Scop versus after, $t_{(5)} = 0.1843$, $p = 0.8610$; before versus after, $t_{(5)} = 1.195$, $p = 0.2858$. ***J***, Schematic diagram of the *in vivo* calcium imaging experiments involving pharmacology or RNAi. ***K–N***, A 30° × 64° motion-defined bar evoked visual responses in R neurons that were blocked by 50 μM Meca (***K***), but not by 50 μM Scop (***M***). The bar moved at 40°/s from ipsi to contra. The gray-shaded regions represent duration of stimulation (2.5 s). The results of the statistical analysis are as indicated (***L***, ***N***). For Meca treatment, $n = 6$ flies. Before versus Meca, Wilcoxon matched-pairs signed-rank test, $W = 21$, $p = 0.0313$; Meca versus after, two-tailed paired t test, $t_{(5)} = 3.293$, $p = 0.0216$. Before versus after, Wilcoxon matched-pairs signed-rank test, $W = 21$, $p = 0.0313$. For Scop treatment, $n = 6$ flies. Two-tailed paired t tests were used in all comparisons. Before versus Scop, $t_{(5)} = 0.4418$, $p = 0.6771$; Scop versus after, $t_{(5)} = 0.1173$, $p = 0.9112$; before versus after, $t_{(5)} = 0.1281$, $p = 0.7898$. ***O***, ***P***, Downregulating the expression

tracking behavior. To explore this behavior, we genetically silenced the R (R20A02-GAL4) or TuBu (R48B06-GAL4) neurons by expressing Kir2.1, an inwardly rectifying potassium channel (Baines et al., 2001). Rigid-tethered flies were confronted with a 30° × 90° luminance- or motion- defined bar oscillating between ±90°, and their real-time steering trajectories were recorded (Fig. 6*A*). We initially examined whether Kir2.1 was expressed in the VNC of blocked flies as previous studies have demonstrated that neck, wing, or haltere neuropils of the VNC are responsible for motor control (Court et al., 2020; Phelps et al., 2021). Immunostaining results showed that R20A02-GAL4 had little expression in the relevant neuropils (Fig. 6*B*). In contrast, R48B06-GAL4 targeted a portion of neurons that probably innervated the wing neuropil of the VNC (Fig. 6*C*). Thus, Tsh-GAL80 was used to further exclude the interference of these neurons in the VNC for testing behavior (Fig. 6*D*).

To evaluate the behavioral performance of flies, the correlation between their steering trajectories and bar positions during the entire stimulation period was calculated. We found that blocking R or TuBu neurons had no effects on the correlation as a luminance-defined bar sweeping across the screen (Fig. 6*E–I*). The behavioral responses of R-blocked flies were not significantly different from those of the UAS control flies, although they did show slight differences from the GAL4 control flies (Fig. 6*F*,*G*). The responses of TuBu-blocked flies did not show significant differences from either control flies (Fig. 6*H*,*I*). In contrast, the inactivation of R or TuBu neurons impaired the tracking behavior of flies in response to a motion-defined bar (Fig. 6*J–N*). In comparison with both parental control groups, bocking R neurons (Fig. 6*K*,*L*) or TuBu neurons (Fig. 6*M*,*N*) significantly reduced the correlations. To further compare the variability between the trajectories of blocked and control flies, we measured the SDs of trajectories within each fly group during the presentation of the motion-defined bar. Throughout the majority of the simulation period, the SDs in R-blocked flies were larger than those in both control groups (Fig, 6*O*; R-blocked greater than UAS control, 86.25%; R-blocked greater than GAL4 control, 80%), which resulted in a significantly increased variances in steering trajectories (Fig. 6*P*). Similarly, when TuBu neurons were blocked, we observed behavioral responses with larger SDs compared with control flies during most of the stimulation period (Fig, 6*Q*; TuBu-blocked greater than UAS control, 78.25%; TuBu-blocked greater than GAL4 control, 82.5%). Statistically, the variances in steering trajectories of TuBu-blocked flies were significantly increased, compared with both control flies (Fig. 6*R*).

Overall, our results support the hypothesis that normal tracking behavior in response to a motion-defined bar requires a complete visual pathway from TuBu to R neurons. The distinct behavioral responses elicited by a motion- and luminance-defined bar further indicate different visual pathway for flies when confronted with different visual features.

R4d neurons are involved in the encoding and tracking of a motion-defined bar

We found that the microglomeruli of R neurons that responded to motion-defined bars were preferentially located within the dorsolateral part of the superior bulb, where the dendrites of R4d neurons innervate (Hulse et al., 2021). Hence, we examined whether R4d neurons encode a motion-defined bar. c232-GAL4 was used, which has been reported to exclusively target R4d neurons in the superior bulb (Seelig and Jayaraman, 2013). Although R3 neurons were labeled with the same driver line, these two subtypes were distinguished and identified clearly, as labeled R4d and R3 microglomeruli were located in the superior and inferior bulbs, respectively (Fig. 7*A*,*B*). No expression was detected in VNC (Fig. 7*A*). The presentation of a motion-defined bar evoked calcium increases in R4d neurons, which showed no directional selectivity (Fig. 7*C*,*D*, green; 28 ROIs in 7 flies). R3 neurons did not show any calcium changes (Fig. 7*C*,*D*, pink; 46 ROIs in 7 flies). In addition, a small portion of c232-labeled R4d microglomeruli did not respond to the motion-defined bar (Fig. 7*C*,*D*, orange; 10 ROIs in 7 flies). These results corroborate our conclusion that the superior bulb, not the inferior bulb, of R neurons encode the motion-defined bar. To further characterize the visual response properties of R4d neurons labeled by c232-GAL4, the receptive fields were mapped. The receptive fields of responsive R4d neurons covered the ipsilateral visual hemisphere and were localized near the midline of the display (Fig. 7*E*; major axis, 33.9° ± 7.5°; minor axis, 19.5° ± 1.5°).

We next investigated whether R4d neurons are involved in the bar tracking behavior. We blocked the c232-labeled R3/R4d neurons by expressing the tetanus toxin light chain (Sweeney et al., 1995) because the expression of Kir2.1 was lethal for the experimental flies. The R3/R4d-blocked flies showed more chaotic tracking trajectories compared with those of both control flies (Fig. 7*F*), resulting in significant decreased correlations (Fig. 7*G*) and increased variances (Fig. 7*H*,*I*). In comparison with control flies, R3/R4d-blocked flies exhibited behavioral responses with larger SDs during most of the stimulation period (Fig. 7*H*; R3/R4d-blocked greater than UAS control, 82.5%; R3/R4d-blocked greater than GAL4 control, 85%).

Together, the behavioral results combined with the physiological results suggest that c232-labeled R4d neurons contribute to the bar tracking behavior. These results demonstrate that c232-labeled R4d neurons play an essential role in the encoding and tracking of a motion-defined bar and further support the calcium imaging results that the superior, not the inferior R neurons, are sensitive to the motion-defined bar.

Discussion

The central brain of *Drosophila* plays a vital role in visual feature encoding and visually guided behaviors. Here, we revealed that neural circuits projecting from TuBu to R neurons in the superior bulb are sensitive to high-frequency motion-defined bars. We also identified that signal transmission from $TuBu_s$ is mediated by nAChR in superior R neurons, and we demonstrated that the visual pathway is involved in the bar-tracking behavior of rigid-tethered flies. Moreover, the physiological and behavioral experiments using restricted lines suggest that R4d neurons in the superior bulb are required in the tracking of a motion-defined bar. Our findings provide new insights into the representation of motion-defined targets in the central brain and their roles in visually guided behaviors.

←

level of nAChR Dα1 or Dα6 subunit in R neurons significantly reduced their calcium responses to a 30° × 64° motion-defined bar moving at 40°/s. Control (UAS-GCaMp6s/+; R20A02-GAL4/+), n = 10 ROIs in 5 flies. α1 RNAi (UAS-GCaMP6s/+; R20A02-GAL4/UAS-nAChRα1 RNAi), n = 9 ROIs in 5 flies. α6 RNAi (UAS-GCaMP6s/UAS-nAChRα6 RNAi; R20A02-GAL4/+), n = 9 ROIs in 5 flies. Unpaired t tests were used to compare the responses between the RNAi groups and the control group. Control versus α1 RNAi, $t_{(17)} = 2.99$, $p = 0.008$. Control versus α6 RNAi, $t_{(17)} = 2.59$, $p = 0.02$. $^{**}p < 0.01$, $^{*}p < 0.05$.

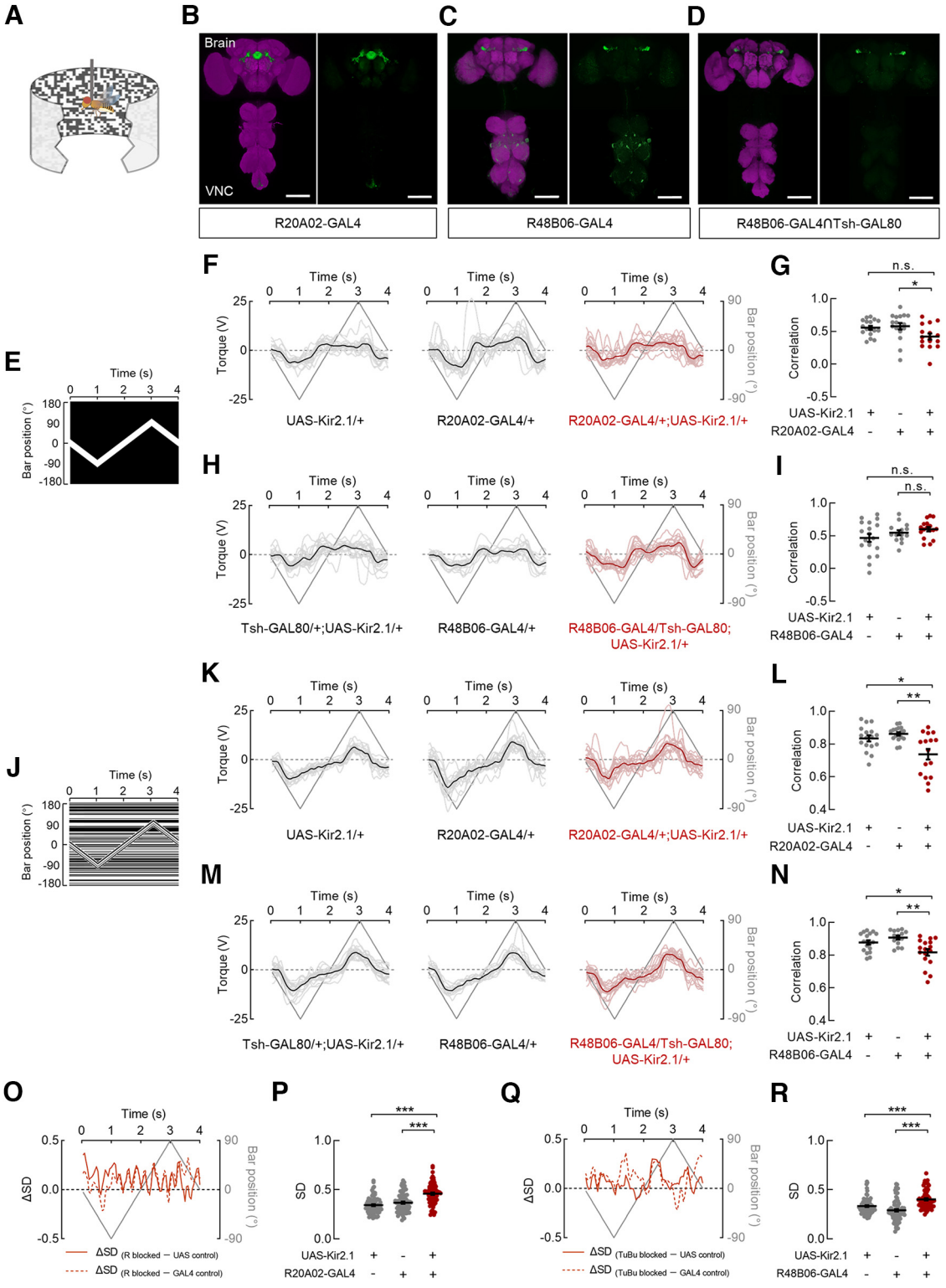

Figure 6. Ring and tuberculo-bulbar neurons are involved in the tracking response toward a motion-defined bar. ***A***, Schematic diagram of the flight simulator. A rigid-tethered fly was surrounded by a panoramic arena. ***B–D***, Anatomy of neurons in the brain and VNC that were labeled by distinct GAL4 lines driving the expression of UAS-Kir2.1::GFP. The following driver lines were used: R20A02-GAL4 (***B***), R48B06-GAL4 (***C***), and R48B06-GAL4∩Tsh-GAL80 (***D***). Neuropil was immunostained with anti-Bruchpilot (magenta). Scale bars, 100 μm. ***E***, The space–time plot for a 30° × 90° luminance-defined bar. The bar started at the center (0°) of the arena and oscillated between ± 90° at 90°/s. ***F***, Steering trajectories of R-blocked flies and both parental control flies in response to the luminance-defined bar. UAS-Kir2.1/+ (left), $n = 17$ flies; R20A02-GAL4/+ (middle), $n = 17$ flies; R20A02-GAL4/+; UAS-Kir2.1/+ (right), $n = 16$ flies. Lines in deep gray indicate the bar position. Lines in black or deep red represent the mean responses of all flies. An individual line in gray or light red represents the trial-averaged response from a single fly. ***G***, The correlations between steering trajectories and bar positions for all flies in ***F***. The correlations in R-blocked flies were significantly different from those in the GAL4 control but not in the UAS control. Kruskal–Wallis test with Dunn's multiple comparisons test, $H = 7.99$, $p = 0.0184$. GAL4 control versus blocked flies, $p = 0.0183$; UAS control versus blocked flies, $p = 0.1363$. Black lines indicate mean ± SEM across flies. ***H***, Steering trajectories of TuBu-blocked flies and both parental control flies in response to the luminance-defined bar. Tsh-GAL80/+; UAS-Kir2.1/+, $n = 18$ flies; R48B06-GAL4/+; UAS-Kir2.1/+, $n = 14$ flies; R48B06-GAL4/Tsh-GAL80; UAS-Kir2.1/+, $n = 17$ flies. ***I***, The correlations between steering trajectories and bar positions for all flies in ***H***. The correlations in TuBu-blocked flies were not significantly different from those in both parental control flies. Brown–Forsythe ANOVA with Tamhane's test, $F_{(2,36.1)} =$

Microglomeruli in the superior and inferior bulbs are thought to represent different information (Omoto et al., 2017; Shiozaki and Kazama, 2017; Hardcastle et al., 2021). Our findings in the present study provide compelling evidence for such a functional difference. First, a luminance-defined bar was able to evoke excitatory or inhibitory responses in inferior R neurons, whereas it only activated superior R neurons. The variable responses of the inferior R neurons indicate that within the R3d/m/p populations there are two different functional subtypes that carry diverse signals. A recently published *Drosophila* connectome, which suggested that different subtypes of R3 neurons receive distinct inputs, might support this hypothesis (Scheffer et al., 2020; Hulse et al., 2021). Second, a motion-defined bar elicited robust excitation in a small population of superior R neurons, but no calcium changes in the inferior R neurons. Anatomical studies have classified eight subtypes of R neurons in the superior bulb (Hulse et al., 2021). Here, we identify that R4d neurons are most likely the population that is sensitive to a motion-defined bar. In contrast, another visually responsive subtype, R2 neurons, might respond to a luminance-defined bar in our study or to polarized light as shown in a previous study (Hardcastle et al., 2021). Whether other superior neurons, including R3w and R5 neurons, sense the visual information is still unknown. Finally, the responses of upstream TuBu neurons to a motion-defined bar resembled those of R neurons. Previous studies have demonstrated that $TuBu_s$ neurons encode polarization signals, whereas $TuBu_i$ neurons do not (Hardcastle et al., 2021). Here, we showed that $TuBu_s$ neurons also transmitted the visual features of a motion-defined bar, whereas the $TuBu_i$ neurons did not. Together, we provide direct physiological and behavioral evidence to support a functional division of the superior and inferior bulbs, indicating that the neural mechanisms for luminance- and motion-defined bars representation are partially separated in the central brain.

Our work identified that a subpopulation of $TuBu_s$ neurons transmitted information regarding motion-defined bars to superior R neurons. Previous studies have reported that the visual responses of superior R neurons to a luminance-defined bar also originate from upstream $TuBu_s$ neurons (Sun et al., 2017). Might it be possible that these two kinds of visual signals originate from different inputs to a single $TuBu_s$ neuron? There are primarily two classes of neurons that provide inputs to TuBu neurons: MeTu (Medullo-Tubercular) and AOTU046 (or VBT) neurons (Scheffer et al., 2020; Tai et al., 2021). MeTu neurons are demonstrated to respond to luminance-defined stimuli and polarized light (Hardcastle et al., 2021), whereas the visual property of VBT neurons remains unknown. These studies suggest that $TuBu_s$ neurons may receive motion- and luminance-defined visual signals from distinct inputs. Moreover, some visual projection neurons in the lobula complex show a unique preference for a luminance- or motion-defined bar (Aptekar et al., 2015; Wu et al., 2016; Städele et al., 2020). We therefore hypothesize that these visual features may be segregated early at the level of the peripheral visual system (before the AOTU) and then converge in $TuBu_s$ neurons.

In the bulb neuropil, TuBu neurons and their downstream R neurons form spatially restricted synaptic connections (Hulse et al., 2021). Our study demonstrate that the calcium and behavioral responses are quite similar between $TuBu_s$ and superior R neurons, which indicates that the function of their synapses might be a relay of visual information. Furthermore, we hypothesize that a population coding mechanism is able to resolve the visual discrimination in the neuronal networks within the bulb. Of the R neuron subtypes, R2 and R4d neurons in the superior bulb, R3m/p neurons in the inferior bulb, and R4m neurons in the anterior bulb have been reported visually responsive (Seelig and Jayaraman, 2013; Shiozaki and Kazama, 2017; Sun et al., 2017; Hardcastle et al., 2021). It is noteworthy that the same subtype of R neurons can be activated by multiple visual features, for instance, R2 and R4m neurons multiplexes polarized and unpolarized light signals (Hardcastle et al., 2021). Our results demonstrate that R4d neurons are activated by both motion- and luminance-defined stimuli. Consequently, it is unlikely that different visual features are discriminated through one specific subtype of R neurons. Instead, our data suggest that motion- and luminance-defined bars could be distinguished by ensemble activities of superior and inferior R neurons. When motion-defined bars are displayed, R4d neurons in the superior bulb are activated, and the activities of inferior R neurons remain unchanged. In contrast, R neurons in both the superior and inferior bulbs respond to the presentation of luminance-defined bars. The diverse visual features delivered from the peripheral visual system could be transformed into a reduced representation via population coding strategies of R neurons, enabling flexible encoding in the central brain.

As a multisensory and motor center, R neurons express several kinds of neurotransmitter receptors for integrating external sensory cues and modulating outputs. Excitatory inputs from NMDA and 5-HT receptors have previously been demonstrated to regulate circadian rhythms (Nichols, 2007; S. Liu et al., 2016; C. Liu et al., 2019; Raccuglia et al., 2019). GABA inhibition among R neurons plays a critical role in promoting copulation (Ishimoto and Kamikouchi, 2020). Dopaminergic signaling to R

←

2.221, $p = 0.1231$. GAL4 control versus blocked flies, $p = 0.6686$; UAS control versus blocked flies, $p = 0.1937$. ***J***, The space–time plot for a 30° × 90° motion-defined bar. The bar started at the center (0°) of the arena and oscillated between ± 90° at 90°/s. ***K***, Steering trajectories of R-blocked flies and both parental control flies in response to the motion-defined bar. UAS-Kir2.1/+, $n = 17$ flies; R20A02-GAL4/+, $n = 17$ flies; R20A02-GAL4/+; UAS-Kir2.1/+, $n = 16$ flies. ***L***, The correlations between steering trajectories and bar positions for all flies in ***K***. The correlations in R-blocked flies were significantly lower than those in both parental control flies. Brown–Forsythe ANOVA with Tamhane's test, $F_{(2,28.08)} = 8.478$, $p = 0.0013$. GAL4 control versus blocked flies, $p = 0.0054$; UAS control versus blocked flies, $p = 0.0458$. ***M***, Steering trajectories of TuBu-blocked flies and both parental control flies in response to the motion-defined bar. Tsh-GAL80/+; UAS-Kir2.1/+, $n = 18$ flies; R48B06-GAL4/+; UAS-Kir2.1/+, $n = 14$ flies; R48B06-GAL4/Tsh-GAL80; UAS-Kir2.1/+, $n = 17$ flies. ***N***, The correlations between steering trajectories and bar positions for all flies in ***M***. The correlations in TuBu-blocked flies were significantly lower than those in both parental control flies. One-way ANOVA with Tukey's test, $F_{(2,46)} = 7.802$, $p = 0.0012$. GAL4 control versus blocked flies, $p = 0.0011$; UAS control versus blocked flies, $p = 0.0249$. ***O***, The differences in the SD of steering trajectories between R-blocked flies and both control flies (solid line, UAS control; dotted line, GAL4 control) throughout the duration when a motion-defined bar was presented. Values > 0 represent the time intervals in which the steering trajectories in R-blocked flies had larger SDs compared with control groups. ***P***, Comparisons of SDs between R-blocked flies and both parental control flies. The SDs in R-blocked flies were significantly larger than those in control flies; $n = 80$ data points in each group. Kruskal–Wallis test with Dunn's multiple comparisons test, $H = 51.14$, $p < 0.0001$. GAL4 control versus blocked flies, $p < 0.0001$; UAS control versus blocked flies, $p < 0.0001$. ***Q***, The differences in the SD of steering trajectories between TuBu-blocked flies and both control flies throughout the duration when a motion-defined bar was presented. Values > 0 represent the time intervals in which the steering trajectories in TuBu-blocked flies had larger SDs compared with control groups. ***R***, Comparisons of SDs between TuBu-blocked flies and both parental control flies. The SDs in TuBu-blocked flies were significantly larger than those in control flies; $n = 80$ data points in each group. Kruskal–Wallis test with Dunn's multiple comparisons test, $H = 54.93$, $p < 0.0001$. GAL4 control versus blocked flies, $p < 0.0001$; UAS control versus blocked flies, $p < 0.0001$. ***$p < 0.001$, **$p < 0.01$, *$p < 0.05$.

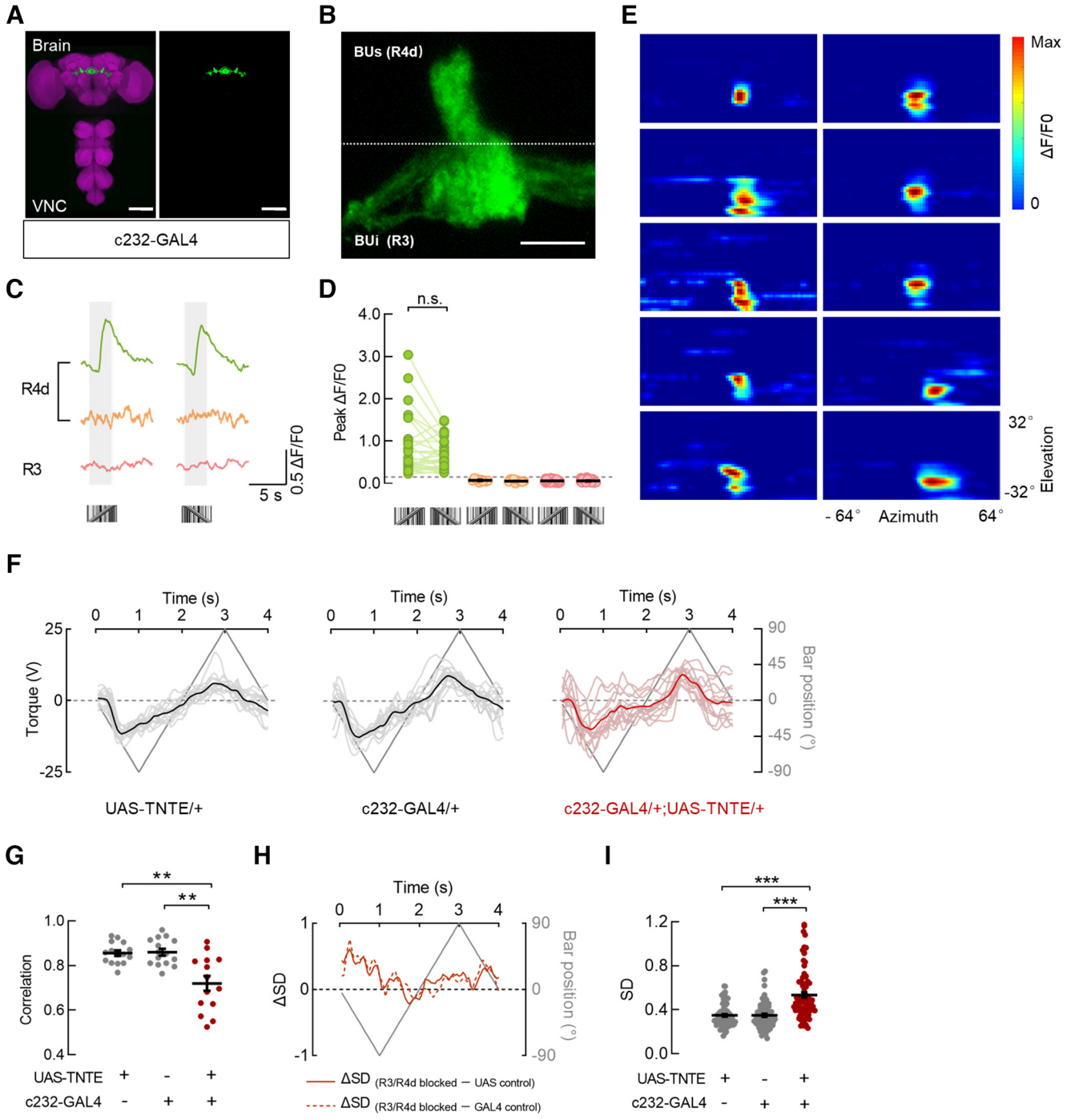

Figure 7. R4d neurons participate in the encoding and tracking of a motion-defined bar. ***A***, Anatomy of neurons in the brain and VNC that were labeled by c232-GAL4 driving the expression of UAS-mCD8::GFP. Neuropil was immunostained with anti-Bruchpilot (magenta). Scale bars, 100 μm. ***B***, The drive line in ***A*** targeted R4d neurons that innervate the dorsolateral part of the superior bulb (BUs) and R3 neurons that innervate the inferior bulb (BUi). Scale bar, 10 μm. ***C***, Calcium responses of three example microglomeruli of R neurons to 30° × 64° motion-defined bars moving at 40°/s. An example R4d microglomerulus responded to a motion-defined bar in both directions (green), whereas another R4d microglomerulus did not (orange). The example R3 microglomerulus did not respond to motion-defined bars (pink). The gray-shaded regions represent duration of stimulation (2.5 s). ***D***, Peak responses of all recorded R4d (green and orange) and R3 (pink) neurons from seven flies to a motion-defined bar in both directions. Green dots, $n = 28$ ROIs; orange dots, $n = 10$ ROIs; pink dots, $n = 46$ ROIs. ROIs with the same color showed homogeneous visual responses, n.s., Wilcoxon matched-pairs signed-rank test, $W = 144$, $p = 0.1042$. Black lines indicate mean ± SEM across microglomeruli. ***E***, Receptive field maps for microglomeruli of R4d neurons that were responsive to motion-defined bars; $n = 10$ ROIs in 5 flies. ***F***, Steering trajectories of flies with distinct genotypes. UAS-TNTE/+ (left), $n = 15$ flies; c232-GAL4/+ (middle), $n = 15$ flies; c232-GAL4/+; UAS-TNTE/+ (right), $n = 14$ flies. Lines in deep gray indicate the bar position. Lines in black or deep red represent the mean responses of all flies. An individual line in gray or light red represents the trial-averaged response from a single fly. ***G***, The correlations between steering trajectories and bar positions for all flies in ***F***. The correlations in R3/R4d-blocked flies were significantly lower than those in both parental control flies. Brown–Forsythe ANOVA with Tamhane's test, $F_{(2,22.5)} = 12.38$, $p = 0.0002$. GAL4 control versus blocked flies, $p = 0.0039$; UAS-control versus blocked flies, $p = 0.0047$. Black lines indicate mean ± SEM across flies. ***H***, The differences in the SD of steering trajectories between R3/R4d-blocked flies and both control flies (solid line, UAS control; dotted line, GAL4 control) throughout the duration when a motion-defined bar was presented. Values > 0 represent the time intervals in which the steering trajectories in R3/R4d-blocked flies had larger SDs compared with control groups. ***I***, Comparisons of SDs between R3/R4d-blocked flies and both parental control flies. The SDs in R3/R4d-blocked flies were significantly larger than those in control flies; $n = 80$ data points in each group. Kruskal–Wallis test with Dunn's multiple comparisons test, $H = 52.64$, $p < 0.0001$. GAL4 control versus blocked flies, $p < 0.0001$; UAS control versus blocked flies, $p < 0.0001$. ***$p < 0.001$.

neurons is indispensable to motor coordination (Kottler et al., 2019). Although many studies have investigated the participation of R neurons in visually guided behaviors, the underlying neurotransmission remains poorly understood. Here, we revealed that nAChR contributes to visual signaling from $TuBu_s$ neurons to superior R neurons, highlighting their role in the motion vision. In the vertebrate visual cortex, cholinergic signaling is incorporated into visual sensory enhancement (Groleau et al., 2015), which suggests that an analog in flies might improve the discrimination of a motion-defined bar. However, we cannot rule out the possibility that other transmitters might also be incorporated into the visual pathway. Nonetheless, our results broaden our knowledge of the way the central brain guides multiple behaviors that rely on diverse chemical signaling systems.

When the normal function of TuBu or R neurons was altered, impaired tracking responses were observed to a motion-defined bar but not to a luminance-defined bar. The behavioral effects on the motion-defined bar tracking behavior are within our expectation from the calcium imaging results, further supporting that superior TuBu and R neurons are actively encoding a high-frequency spatial feature. In contrast, the TuBu−R pathway does not appear to be involved in the luminance-defined bar tracking, although the majority of TuBu and R neuron subtypes showed a preference for a low-frequency solid ON bar. The distinct behavioral effects highlight a functional role of superior TuBu and R neurons in discriminating motion-defined features. These neurons with no directional selectivity may enhance the overall discrimination of high spatial frequency information within the motion-defined bar and work in conjunction with motion direction detectors, thereby enabling the downstream circuits to generate appropriate directional flight steering commands.

However, both TuBu- and R-blocked flies showed remaining tracking responses to motion-defined bars. These results indicate that alternative visual pathways contribute to bar tracking behavior, which is likely important for behavioral stability. Visually responsive neurons in the lobula complex that have no direct connection with the central complex are potential alternatives (Aptekar et al., 2015; Städele et al., 2020). Another possible explanation for the remaining tracking behavior is that in the case of population coding, the driver lines we used targeted only a portion of the relevant neurons. Moreover, the discrepancy of the behavioral effects when neurons were silenced with distinct driver lines might be because they targeted different populations of the relevant neurons. Considering the remarkable ability of flies to track a motion-defined bar, a more detailed analysis of the functional visual pathway is warranted.

In conclusion, we identified the neural correlates for the representation of motion-defined bars in the central brain and highlighted the essential roles of TuBu and R neurons in visually guided behaviors. Moreover, R neurons innervating the superior and inferior bulb domains were revealed to show distinct response patterns to motion- and luminance-defined bars. These results suggest that the bulb might act as a portal for external sensory information flowing into the central complex, with visual features segregated by functionally distinct circuits. Our findings provide new directions for investigating the function of the central complex in sensory-motor transformation.

References

Aptekar JW, Keleş MF, Lu PM, Zolotova NM, Frye MA (2015) Neurons forming optic glomeruli compute figure-ground discriminations in *Drosophila*. J Neurosci 35:7587–7599.

Bahl A, Ammer G, Schilling T, Borst A (2013) Object tracking in motion-blind flies. Nat Neurosci 16:730–738.

Baines RA, Uhler JP, Thompson A, Sweeney ST, Bate M (2001) Altered electrical properties in *Drosophila* neurons developing without synaptic transmission. J Neurosci 21:1523–1531.

Barlow HB, Levick WR (1965) The mechanism of directionally selective units in rabbit's retina. J Physiol 178:477–504.

Court R, Namiki S, Armstrong JD, Börner J, Card G, Costa M, Dickinson M, Duch C, Korff W, Mann R, Merritt D, Murphey RK, Seeds AM, Shirangi T, Simpson JH, Truman JW, Tuthill JC, Williams DW, Shepherd D (2020) A systematic nomenclature for the *Drosophila* ventral nerve cord. Neuron 107:1071–1079.e2.

Euler T, Detwiler PB, Denk W (2002) Directionally selective calcium signals in dendrites of starburst amacrine cells. Nature 418:845–852.

Fenk LM, Poehlmann A, Straw AD (2014) Asymmetric processing of visual motion for simultaneous object and background responses. Curr Biol 24:2913–2919.

Fisher YE, Lu J, D'Alessandro I, Wilson RI (2019) Sensorimotor experience remaps visual input to a heading-direction network. Nature 576:121–125.

Groleau M, Kang JI, Huppé-Gourgues F, Vaucher E (2015) Distribution and effects of the muscarinic receptor subtypes in the primary visual cortex. Front Synaptic Neurosci 7:10.

Hanesch U, Fischbach K-F, Heisenberg M (1989) Neuronal architecture of the central complex in *Drosophila melanogaster*. Cell Tissue Res 257:343–366.

Hardcastle BJ, Omoto JJ, Kandimalla P, Nguyen BM, Keleş MF, Boyd NK, Hartenstein V, Frye MA (2021) A visual pathway for skylight polarization processing in *Drosophila*. Elife 10:e63225.

Hulse BK, Haberkern H, Franconville R, Turner-Evans DB, Takemura SY, Wolff T, Noorman M, Dreher M, Dan C, Parekh R, Hermundstad AM, Rubin GM, Jayaraman V (2021) A connectome of the *Drosophila* central complex reveals network motifs suitable for flexible navigation and context-dependent action selection. Elife 10:e66039.

Ishimoto H, Kamikouchi A (2020) A feedforward circuit regulates action selection of pre-mating courtship behavior in female *Drosophila*. Curr Biol 30:396–407.e4.

Ji X, Yuan D, Wei H, Cheng Y, Wang X, Yang J, Hu P, Gestrich JY, Liu L, Zhu Y (2020) Differentiation of theta visual motion from Fourier motion requires LC16 and R18C12 neurons in Drosophila. iScience 23:101041.

Joesch M, Schnell B, Raghu SV, Reiff DF, Borst A (2010) ON and OFF pathways in *Drosophila* motion vision. Nature 468:300–304.

Kottler B, Faville R, Bridi JC, Hirth F (2019) Inverse control of turning behavior by dopamine D1 receptor signaling in columnar and ring neurons of the central complex in *Drosophila*. Curr Biol 29:567–577.e6.

Kuntz S, Poeck B, Sokolowski MB, Strauss R (2012) The visual orientation memory of *Drosophila* requires Foraging (PKG) upstream of Ignorant (RSK2) in ring neurons of the central complex. Learn Mem 19:337–340.

Leiss F, Koper E, Hein I, Fouquet W, Lindner J, Sigrist S, Tavosanis G (2009) Characterization of dendritic spines in the *Drosophila* central nervous system. Dev Neurobiol 69:221–234.

Liu C, Meng Z, Wiggin TD, Yu J, Reed ML, Guo F, Zhang Y, Rosbash M, Griffith LC (2019) A serotonin-modulated circuit controls sleep architecture to regulate cognitive function independent of total sleep in *Drosophila*. Curr Biol 29:3635–3646.e5.

Liu S, Liu Q, Tabuchi M, Wu MN (2016) Sleep drive is encoded by neural plastic changes in a dedicated circuit. Cell 165:1347–1360.

Mauss AS, Vlasits A, Borst A, Feller M (2017) Visual circuits for direction selectivity. Annu Rev Neurosci 40:211–230.

Nichols CD (2007) 5-HT2 receptors in *Drosophila* are expressed in the brain and modulate aspects of circadian behaviors. Dev Neurobiol 67:752–763.

Ofstad TA, Zuker CS, Reiser MB (2011) Visual place learning in *Drosophila melanogaster*. Nature 474:204–207.

Omoto JJ, Keleş MF, Nguyen BM, Bolanos C, Lovick JK, Frye MA, Hartenstein V (2017) Visual input to the *Drosophila* central complex by developmentally and functionally distinct neuronal populations. Curr Biol 27:1098–1110.

Omoto JJ, Nguyen BM, Kandimalla P, Lovick JK, Donlea JM, Hartenstein V (2018) Neuronal constituents and putative interactions within the *Drosophila* ellipsoid body neuropil. Front Neural Circuits 12:103.

Pan Y, Zhou Y, Guo C, Gong H, Gong Z, Liu L (2009) Differential roles of the fan-shaped body and the ellipsoid body in *Drosophila* visual pattern memory. Learn Mem 16:289–295.

Phelps JS, Hildebrand DGC, Graham BJ, Kuan AT, Thomas LA, Nguyen TM, Buhmann J, Azevedo AW, Sustar A, Agrawal S, Liu M, Shanny BL, Funke J, Tuthill JC, Lee W-CA (2021) Reconstruction of motor control circuits in adult *Drosophila* using automated transmission electron microscopy. Cell 184:759–774.e18.

Raccuglia D, Huang S, Ender A, Heim MM, Laber D, Suárez-Grimalt R, Liotta A, Sigrist SJ, Geiger JRP, Owald D (2019) Network-specific synchronization of electrical slow-wave oscillations regulates sleep drive in *Drosophila*. Curr Biol 29:3611–3621.e3.

Regan D, Beverley KI (1984) Figure–ground segregation by motion contrast and by luminance contrast. J Opt Soc Am A 1:433–442.

Reichardt W, Poggio T (1979) Figure and ground discrimination by relative movement in the visual system of the fly. Biol Cybern 45:63–70.

Scheffer LK, et al. (2020) A connectome and analysis of the adult *Drosophila* central brain. Elife 9:e57443.

Seelig JD, Jayaraman V (2013) Feature detection and orientation tuning in the *Drosophila* central complex. Nature 503:262–266.

Shiozaki HM, Kazama H (2017) Parallel encoding of recent visual experience and self-motion during navigation in *Drosophila*. Nat Neurosci 20:1395–1403.

Städele C, Keleş MF, Mongeau JM, Frye MA (2020) Non-canonical receptive field properties and neuromodulation of feature-detecting neurons in flies. Curr Biol 30:2508–2519.e6.

Stevens M, Merilaita S (2009) Animal camouflage: current issues and new perspectives. Philos Trans R Soc Lond B Biol Sci 364:423–427.

Stevens M, Ruxton GD (2019) The key role of behaviour in animal camouflage. Biol Rev Camb Philos Soc 94:116–134.

Sun Y, Nern A, Franconville R, Dana H, Schreiter ER, Looger LL, Svoboda K, Kim DS, Hermundstad AM, Jayaraman V (2017) Neural signatures of dynamic stimulus selection in *Drosophila*. Nat Neurosci 20:1104–1113.

Sweeney ST, Broadie K, Keane J, Niemann H, O'Kane CJ (1995) Targeted expression of tetanus toxin light chain in *Drosophila* specifically eliminates synaptic transmission and causes behavioral defects. Neuron 14:341–351.

Tai C-Y, Chin A-L, Chiang A-S (2021) Comprehensive map of visual projection neurons for processing ultraviolet information in the *Drosophila* brain. J Comp Neurol 529:1988–2013.

Theobald JC, Shoemaker PA, Ringach DL, Frye MA (2010) Theta motion processing in fruit flies. Front Behav Neurosci 4:35.

Wang Z, Pan Y, Li W, Jiang H, Chatzimanolis L, Chang J, Gong Z, Liu L (2008) Visual pattern memory requires foraging function in the central complex of *Drosophila*. Learn Mem 15:133–142.

Wu M, Nern A, Williamson WR, Morimoto MM, Reiser MB, Card GM, Rubin GM (2016) Visual projection neurons in the *Drosophila* lobula link feature detection to distinct behavioral programs. Elife 5:e21022.

Zhang YQ, Rodesch CK, Broadie K (2002) Living synaptic vesicle marker: synaptotagmin-GFP. Genesis 34:142–145.